Anthropogenic air pollution observed near dust source regions in northwestern China during springtime 2008

Can Li,[1,2] Si-Chee Tsay,[2] Joshua S. Fu,[3] Russell R. Dickerson,[1] Qiang Ji,[1,2] Shaun W. Bell,[2,4] Yang Gao,[3] Wu Zhang,[5] Jianping Huang,[5] Zhanqing Li,[1,6,7] and Hongbin Chen[6]

Received 3 December 2009; revised 28 May 2010; accepted 10 June 2010; published 13 October 2010.

[1] Trace gases and aerosols were measured in Zhangye (39.082°N, 100.276°E, 1460 m a.s.l.), a rural site near the Gobi deserts in northwestern China during spring 2008. Primary trace gases (CO: 265 ppb; SO_2: 3.4 ppb; NO_y^*: 4.2 ppb; hereafter results given as means of hourly data) in the area were lower than in eastern China, but still indicative of marked anthropogenic emissions. Sizable aerosol mass concentration (153 μg/m^3) and light scattering (159 Mm^{-1} at 500 nm) were largely attributable to dust emissions, and aerosol light absorption (10.3 Mm^{-1} at 500 nm) was dominated by anthropogenic pollution. Distinct diurnal variations in meteorology and pollution were induced by the local valley terrain. Strong daytime northwest valley wind cleaned out pollution and was replaced by southeast mountain wind that allowed pollutants to build up overnight. In the afternoon, aerosols had single scattering albedo (SSA, 500 nm) of 0.95 and were mainly of supermicron particles, presumably dust, while at night smaller particles and SSA of 0.89–0.91 were related to pollution. The diverse local emission sources were characterized: the CO/SO_2, CO/NO_y, NO_y/SO_2 (by moles), and BC/CO (by mass) ratios for small point sources such as factories were 24.6–54.2, 25.8–35.9, 0.79–1.31, and 4.1–6.1 × 10^{-3}, respectively, compared to the corresponding inventory ratios of 43.7–71.9, 23.7–25.7, 1.84–2.79, and 3.4–4.0 × 10^{-3} for the industrial sector in the area. The mixing between dust and pollution can be ubiquitous in this region. During a dust storm shown as an example, pollutants were observed to mix with dust, causing discernible changes in both SSA and aerosol size distribution. Further interaction between dust and pollutants during transport may modify the properties of dust particles that are critical for their large-scale impact on radiation, clouds, and global biogeochemical cycles.

Citation: Li, C., et al. (2010), Anthropogenic air pollution observed near dust source regions in northwestern China during springtime 2008, *J. Geophys. Res.*, *115*, D00K22, doi:10.1029/2009JD013659.

1. Introduction

[2] With the Taklimakan and Gobi deserts sprawling over massive areas in China and Mongolia, East Asia is one of the major source regions of airborne dust in the world [e.g., *Ginoux et al.*, 2001; *Prospero et al.*, 2002; *Tanaka and Chiba*, 2006]. Driven by strong surface winds associated with the midlatitude wave cyclones [e.g., *Kurosaki and Mikami*, 2003; *Qian et al.*, 2002; *Shao and Dong*, 2006; *Sun et al.*, 2001; *Zhu et al.*, 2008], the dust storms in East Asia occur most frequently in spring [e.g., *Yue et al.*, 2009]. They are often of synoptic scale [e.g., *Hsu et al.*, 2006; *Wang et al.*, 2007], and influence large areas from near the deserts [e.g., *Cheng et al.*, 2006; *Fu et al.*, 2008] to the west coast of the Pacific [e.g., *Fang et al.*, 1999; *Lee et al.*, 2006; *Liu et al.*, 2009; *Sun et al.*, 2005]. The long-range transport of Asian dust [e.g., *Duce et al.*, 1980], in some cases across the Pacific, has also been well documented [e.g., *Huang et al.*, 2008; *Husar et al.*, 2001; *Leaitch et al.*, 2009; *McKendry et al.*, 2008; *Zhao et al.*, 2008]. Besides modulating macroscale radiative energy [e.g., *Cheng et al.*, 2006; *Kim et al.*, 2005], and modifying microscale cloud properties [e.g., *Huang et al.*, 2006a, 2006b], Asian dust may also play an important role in the global biogeochemical cycles, as a potential source of iron to the marine ecosystems of the North Pacific [e.g., *Bishop et al.*, 2002; *Gao et al.*, 1997; *Hsu et al.*, 2009; *Zhang and Gao*, 2007].

[1]Earth System Science Interdisciplinary Center, University of Maryland, College Park, Maryland, USA.
[2]NASA Goddard Space Flight Center, Greenbelt, Maryland, USA.
[3]Department of Civil and Environmental Engineering, University of Tennessee, Knoxville, Tennessee, USA.
[4]Science Systems and Applications Inc., Lanham, Maryland, USA.
[5]College of Atmospheric Sciences, Lanzhou University, Lanzhou, China.
[6]Institute of Atmospheric Physics, Chinese Academy of Sciences, Beijing, China.
[7]College of Atmospheric Physics, Nanjing University of Information Science and Technology, Nanjing, China.

Copyright 2010 by the American Geophysical Union.
0148-0227/10/2009JD013659

[3] A key factor determining the large-scale impact of Asian dust is its interaction with various other atmospheric constituents during transport, which for example may mobilize iron in dust particles and make it available to the marine biota [*Meskhidze et al.*, 2005; *Solmon et al.*, 2009]. Black carbon may coat the surface of dust particles and increase their absorption of radiation [e.g., *Chaudhry et al.*, 2007; *Guo et al.*, 2010]. Introduction of compounds such as sulfate and nitrate to dust aerosols can also change their size distribution, optical and hygroscopic properties [e.g., *Carrico et al.*, 2003; *Kelly et al.*, 2007; *Sullivan et al.*, 2009; *Tobo et al.*, 2009; *Zhang and Iwasaka*, 2004], and their lifetime in the atmosphere. Numerical [e.g., *Bian and Zender*, 2003; *Liao et al.*, 2003; *Tang et al.*, 2004; *Zhang et al.*, 1994; *Zhang and Carmichael*, 1999] and laboratory [e.g., *Laskin et al.*, 2005] studies suggest the possibility of heterogeneous reactions taking place on the surface of dust particles, and a number of field experiments have been conducted to provide observational evidence [e.g., *Huebert et al.*, 2003]. Some studies in the industrialized eastern China [e.g., *Huang et al.*, 2010a, 2010b; *Sun et al.*, 2005, 2010; *Yuan et al.*, 2006, 2008; *Wang et al.*, 2007] uncovered that dust and pollution were often mixed coming into the region, while others indicated the two could be separated by frontal systems [e.g., *Guo et al.*, 2004; *Zhang et al.*, 2005]. Traces of chemical modification of dust during transport were found in most experiments farther downwind, off the Chinese coast [e.g., *Arimoto et al.*, 2006; *Gao et al.*, 2007; *Geng et al.*, 2009; *Leaitch et al.*, 2009; *Sullivan et al.*, 2007; *Zhang and Iwasaka*, 2001]. The extent of the modification varies, and could critically depend on the regions the dust plumes travel through, as well as the duration since the mixing occurred between dust and pollutants [e.g., *Maxwell-Meier et al.*, 2004; *Ro et al.*, 2005; *Song et al.*, 2005]. The longer the dust and pollutants stay together, the more thoroughly the composition and properties of dust particles may evolve.

[4] Frequented by dust storms originating from the Taklimakan and Gobi deserts, northwestern China including the arid provinces of Shanxi, Gansu, Ningxia, Xinjiang, and Qinghai (and the western part of Inner Mongolia) is a main source region of airborne Asian dust [e.g., *Laurent et al.*, 2006; *Liu et al.*, 2004; *Shao et al.*, 2003; *Shao and Dong*, 2006; *Xuan et al.*, 2000]. Industry and population in this region experienced substantial growth over the past decade [*National Bureau of Statistics of China*, 2008], leading to large changes in pollutant emissions. For instance, the estimated NO_x emissions from Gansu went up from 195 Gg/yr (10^9 g) in 2000 [*Streets et al.*, 2003] to 323 Gg/yr in 2006 [*Zhang et al.*, 2009], whereas the estimated SO_2 emissions dropped from 439 Gg/yr to 338 Gg/yr. The differences at least partly reflect the actual changes in emissions. The influences of anthropogenic pollution on aerosol composition have been identified in several studies in the region [e.g., *Arimoto et al.*, 2004; *Cao et al.*, 2005; *Li et al.*, 2008a, 2008b; *Shen et al.*, 2009; *Xu et al.*, 2004; *Zhang et al.*, 2003a], but the measurements of aerosol precursor gases are scarce, made mainly in cities and reflect chemical and physical changes that occurred during transport over a variety of environments [e.g., *Chu et al.*, 2008; *Ta et al.*, 2005].

[5] Following a pilot field experiment in 2005 in China under the Eastern Asian Study of Tropospheric Aerosols, an International Regional Experiment (EAST-AIRE) [*Z. Li et al.*, 2007], a more intensive field campaign was conducted in 2008 with multiple extensive observation stations across China, as a part of the joint U.S.-China research endeavor for deploying the Department of Energy's Atmospheric Radiation Measurement (ARM) Mobile Facility (AMF) (Z. Li et al., Overview of the East Asian Study of Tropospheric Aerosols and Impact on Regional Climate (EAST-AIRC), submitted to *Journal of Geophysical Research*, 2010). A suite of surface-based remote sensing and in situ instruments were deployed at the ARM Ancillary Facility consisting of two mobile observatories: SMART (Surface-sensing Measurements of Atmospheric Radiative Transfer) and COMMIT (Chemical, Optical, and Microphysical Measurements of In situ Troposphere), established near the Gobi deserts to study the properties of regional aerosols and their potential climate impact. To our knowledge, this marks the first time such comprehensive observations were made in northwestern China where the dust is generated. In this paper, we analyze the data of trace gases and aerosol properties from the in situ measurements, focusing on the characteristics of air pollution in the area, and its interaction with dust. By exploring a representative dust event observed during the experiment, we demonstrate how anthropogenic pollutants mix with dust, changing the bulk properties of aerosols.

2. Measurements and Ancillary Data

[6] The experiment was carried out from 17 April to 18 June 2008, or day of year (DOY) 108–170, at the Zhangye National Climate Observatory (39.082°N, 100.276°E, 1460 m above sea level) of the China Meteorological Administration, ~20 km northwest of Zhangye, a city of ~300,000 residents in China's northwestern province of Gansu. With the Qilian Mountains (elevation: ~4000 m) to the south and west, and the Beishan Mountains (elevation: ~2000 m) and the Alashan Plateau to the north, Zhangye is one of the several oasis cities scattered along a narrow northwest-southeast-oriented valley stretching ~1000 km in northwestern China, known as the Hexi Corridor (corridor to the west of the Yellow River). The Badain Jaran Desert, part of the Gobi deserts, is merely 100 km to the north, rendering the Hexi Corridor a hot spot of dust storms [e.g., *Shao and Dong*, 2006; *Sun et al.*, 2001]. Airborne dust may also come from the sandy land and the cultivated fields within the valley in April and early May, when little vegetation cover exists prior to the growing season [*Zou and Zhai*, 2004]. The area was dry with a mild temperature throughout the experiment (relative humidity, RH: 28.1 ± 16.2%, temperature: 16.2 ± 7.0°C, mean ± standard deviation).

[7] During the deployment, the SMART-COMMIT observatories were at least 500 m away from any significant anthropogenic emission sources (Figure 1a). The nearest main roadway, the two-lane National Route 312, runs northwest–southeast about 700 m to the north. Several factories were spotted along the road by the authors, including a few sizable ones near Linze, the local township ~7 km to the northwest. A major four-lane highway running east-west is about 8 km to the south. A number of rural residences are scattered around the site, between the two roadways. Overall,

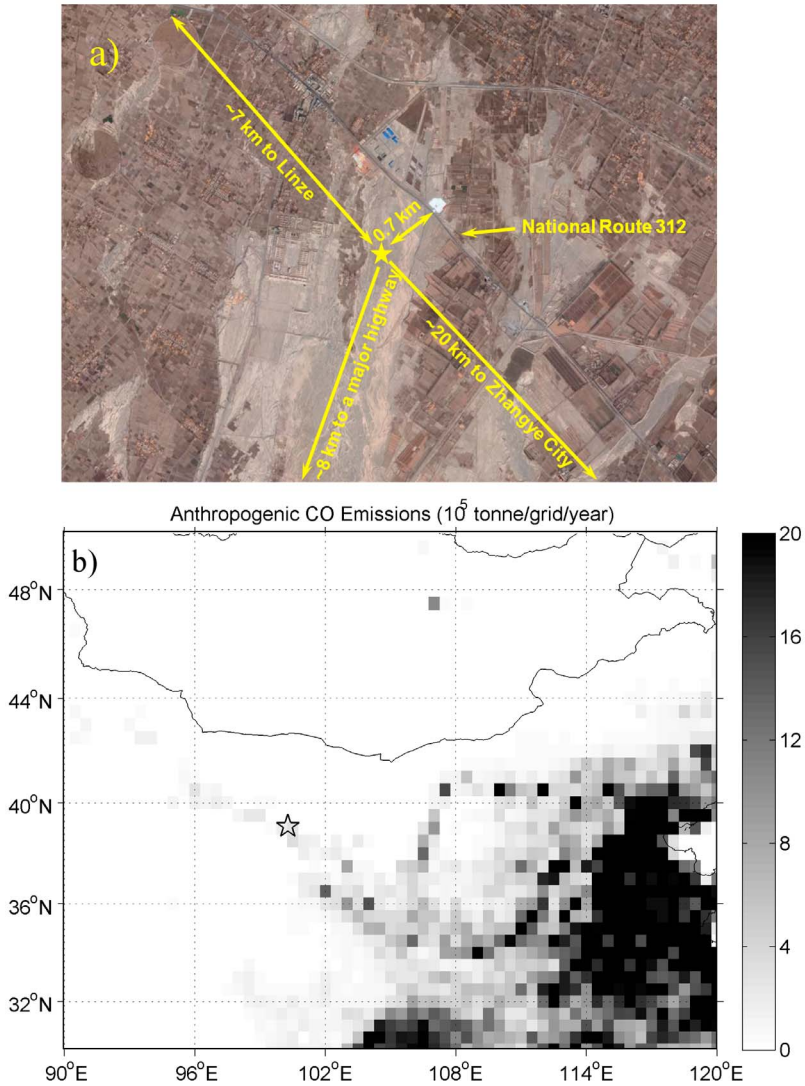

Figure 1. (a) The area surrounding the Zhangye site marked with a star. (b) The estimated anthropogenic CO emissions in 2006 for part of China [*Zhang et al.*, 2009]. The Hexi Corridor is evident in the map as a band of relatively strong emissions extending from (40°N, 96°E) to (36°N, 102°E).

the Hexi Corridor is a relatively populated and polluted region in northwestern China, as evidenced by the estimated CO emissions [*Zhang et al.*, 2009] shown in Figure 1b.

2.1. Trace Gases

[8] All trace gas data were acquired from commercial analyzers manufactured by Thermo Environmental Instruments (TEI), Franklin, MA. A modified [*Dickerson and Delany*, 1988] TEI Model 48C with a detection limit of 35 ppb (signal-to-noise ratio, S:N = 2:1 for $\pm 1\sigma$ noise) for 1 min data was used to measure CO. SO_2 levels were determined with a modified [*Luke*, 1997] TEI Model 43C, which had a detection limit of 0.8 ppb at 1 min resolution (S:N = 2:1 for $\pm 1\sigma$ noise). To measure O_3, we employed a TEI Model 49C, which was calibrated with an in-house primary standard (TEI Model 49 PS) before the experiment and with a transfer standard (TEI Model 146C) afterward. The detection limit was estimated at better than 1 ppb for 1 min averaging time (S:N = 2:1 for $\pm 1\sigma$ noise). A chemiluminescence detector (TEI Model 42C) was used to measure NO, with a detection limit (S:N = 2:1 for $\pm 1\sigma$ noise) of ~0.2 ppb for 1 min data. The TEI 42C also has a hot molybdenum converter to reduce NO_2 prior to detection as NO, and the efficiency was determined by gas-phase titration [e.g., *Dickerson et al.*, 1984]. Such detectors are known to be sensitive to other oxides of nitrogen such as PAN and alkyl nitrates, while HNO_3 is generally lost on the inlet [*Dunlea et al.*, 2007; *Fehsenfeld et al.*, 1987; *Poulida et al.*, 1994]. NO_x is defined as NO + NO_2. NO_y is defined as $NO_x + NO_3 + 2 \times N_2O_5 + HONO + HNO_3 + PAN + RONO_2 + RONO + NO_3^-$. NO_z is defined as $NO_y - NO_x$ [*Seinfeld and Pandis*, 1998]. *Dunlea et al.* [2007] indicate that commercial NO_x monitors detect NO_z with a net efficiency of about 50%, due to the loss of HNO_3 gas to the surface of sampling inlets. Thus the reported nominal NO_x values are in fact an upper limit for NO_x, but a lower limit for NO_y, and we will refer to them as NO_y^*, which are used throughout this paper to qualitatively depict the pollution pattern in the area. For a fraction of the NO_y^* data acquired

under strong influences from local emission sources (spikes in pollutant levels in the morning; see section 3.3), we can make corrections to the NO_y^* data to estimate NO_y concentration, which is used in section 3.3 to characterize those local sources. The correction method is described in section 2.2.

[9] All the trace gas detectors were housed in the COMMIT with temperature control. Sample flows were drawn from the top of the trailer (~4 m above ground) into the instruments through a 3 m long Teflon sampling line. Daily zero checks of all gas instruments were conducted by introducing scrubbed air (TEI Model 146C). In addition, the instrument backgrounds of the CO and SO_2 detectors were determined every few hours. Before, after, and every 3–4 weeks during the deployment, the gas instruments were calibrated with a working standard gas (50.5 ppm CO, 13.5 ppm SO_2, and 10 ppm NO mixed in nitrogen, Scott-Marrin Inc., Riverside, California) traceable to NIST (National Institute of Standards and Technology) standard reference materials, diluted with the TEI Model 146C calibrator. Small nonsystematic changes in the derived calibration factors (within ~15%) suggest that the calibration standards likely remained stable throughout the experiment. Data were stored at 1 min resolution and averaged into 5 min and hourly intervals for this study.

2.2. Correction of the NO_y^* Data

[10] For the morning data, we can estimate the partitioning between NO and NO_2 by assuming the photostationary state [*Leighton*, 1961],

$$\frac{[NO_2]}{[NO]} = \frac{k_{(NO+O_3)}[O_3]_{ss}}{j(NO_2)}, \tag{1}$$

where $k_{(NO+O3)}$ is the rate constant of the reaction $NO + O_3 \rightarrow NO_2 + O_2$, $[O_3]_{ss}$ is the steady state O_3 concentration, and $j(NO_2)$ is the photolysis rate coefficient for NO_2. Note that the oxidation of NO by HO_2 is not considered here, and the actual NO_2/NO ratio could be ~10% greater than estimated with equation (1). We use two methods to calculate $j(NO_2)$, by linking our measured direct and diffuse ultraviolet irradiance for the band of 285–395 nm to $j(NO_2)$ with the relationship proposed by *Madronich* [1987], and by using an empirical equation given by *Dickerson et al.* [1982],

$$j(\mathrm{NO_2}) = 1.67\exp(-0.575\ \sec\theta)\left(\times 10^{-2}\ \mathrm{s}^{-1}\right), \tag{2}$$

where θ is the solar zenith angle. For the first method, we assumed a relatively high albedo of 0.20 (compared to 0.15 used by *Madronich* [1987]) to represent the arid land surface near our site. And the resulted $j(NO_2)$ values are typically ~10–15% greater than those derived from the second method or measured in Boulder, Colorado, a site at similar elevation [e.g., *Shetter et al.*, 2003] for downwelling radiation only.

[11] From the NO concentration and the calculated NO_2/NO ratio, we can then estimate the NO_x concentration. When NO_x is a large fraction of the NO_y^*, the instrument detects NO_y with reasonable precision. In this case, we apply a correction factor of 2 (to account for the 50% detection efficiency) to NO_z, calculated here as the difference between NO_y^* and NO_x estimated using equation (1),

$$\left[\mathrm{NO}_y\right] = [\mathrm{NO}_x] + 2 \times \left(\left[\mathrm{NO}_y^*\right] - [\mathrm{NO}_x]\right). \tag{3}$$

If for example NO_x/NO_y^* is 0.70 then the correction gives a value for $[NO_y]$ equal to 1.3 × $[NO_y^*]$. This correction produces an uncertainty of ~25% in the NO_y values. The NO_y data from the correction are used in section 3.3 to characterize pollutant spikes due to local emission sources.

2.3. Aerosols

[12] The mass concentration of the particulate matter with a diameter of 10 μm or less (PM_{10}) was measured with a TEI Model 1400ab Tapered Element Oscillating Microbalance (TEOM) [*Patashnick and Rupprecht*, 1991]. The minimum detection limit of this instrument is typically 0.06 $\mu g/m^3$ [*Chow et al.*, 2008]. Loss of volatile and semivolatile aerosol compounds due to heating of the sampling stream (50°C) may lead to a negative bias, which should be negligible in the studied environment largely dominated by dust particles.

[13] An integrating nephelometer (TSI Model 3563, Shoreview, MN) measured particle scattering coefficient (B_{sp}) at wavelengths of 450, 550, and 700 nm; the detection limits of the instrument at the three wavelengths are 0.44, 0.17, and 0.26 Mm^{-1} (10^{-6} m^{-1}), respectively (signal-to-noise ratio S:N = 2:1 [*Anderson et al.*, 1996]). The bias related to the nonideal forward-scattering truncation [*Anderson et al.*, 1996] was accounted for, following *Anderson and Ogren* [1998]. The RH reduction due to heat inside the integrating volume is not expected to significantly influence the measured aerosol scattering, since the growth in dust particle size is practically zero under the ambient humidity observed during the experiment.

[14] A seven-wavelength (370, 430, 470, 520, 565, 700, 950 nm) Aethalometer (Magee Scientific Model AE-31, Berkeley, California) monitored the change in transmittance as aerosol particles deposited to a filter tape. The multiple scattering of the filter material and the filter loading effects were accounted for, with the method proposed by *Arnott et al.* [2005], to derive the particle absorption coefficient (B_{ap}). We applied their correcting factors at 520 nm obtained from ambient measurements [*Arnott et al.*, 2005], and extrapolated them to the other wavelengths. Both B_{ap} and B_{sp} measurements were interpolated to the wavelength of 500 nm. We also estimated black carbon (BC) concentration from B_{ap} at 500 nm for local pollutant spikes (see section 3.3), assuming a specific absorption efficiency of 10 m^2/g.

[15] An Aerodynamic Particle Sizer spectrometer (APS, TSI Model 3321) was used to measure the aerodynamic size distribution of particles between 0.5 and 20 μm in diameter, from 17 April until 11 May, before the instrument light source burned out. The performance of the instrument was periodically checked with NIST-traceable monodisperse standards (Duke Scientific, Palo Alto, California). *Peters and Leith* [2003] compared the same model of instrument to an impactor, noticing that the instrument had a low counting efficiency for the total number concentration, but gave a reasonable shape of aerosol size distribution. All aerosol data were available at 5 min and hourly intervals, and reported for volumes under standard conditions (1013.25 hPa and 20°C).

[16] Aerosol samples were pumped through a metal sampling stack (~7 m above the ground level) and conductive tubing, before entering the aerosol instruments in COMMIT. The penetration efficiencies [e.g., *Baron and Willeke*, 2001], calculated assuming particle density of 1000 kg/m^3, are 87% for 20 μm sized particles for the APS, 90% for 10 μm par-

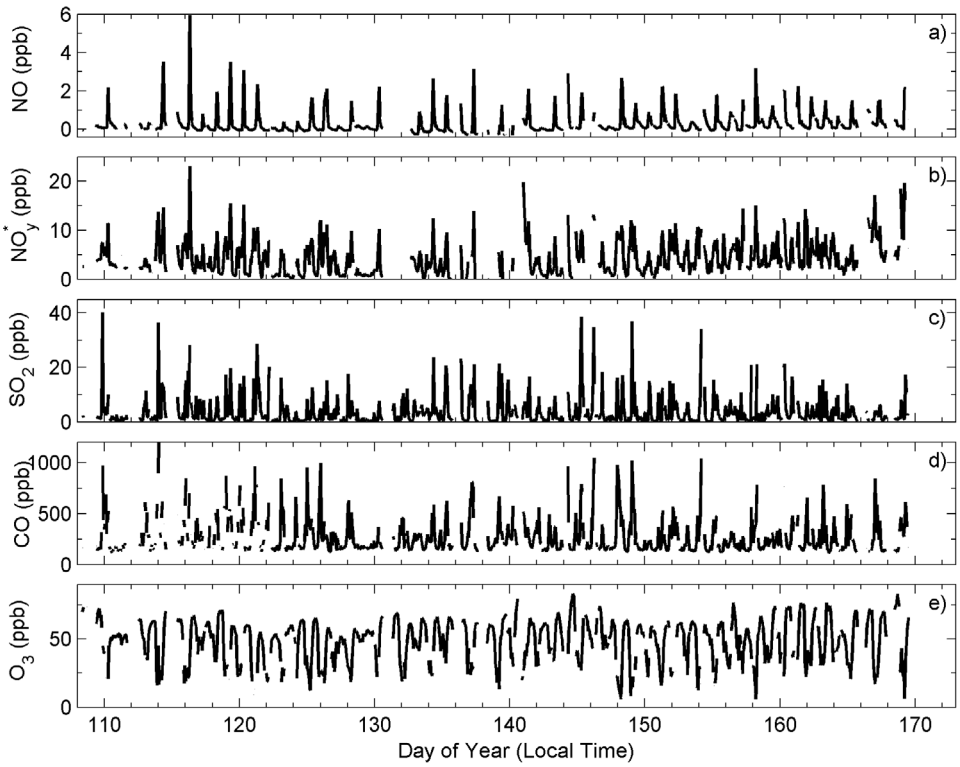

Figure 2. Hourly average concentrations of (a) NO, (b) NO_y^*, (c) SO_2, (d) CO, and (e) O_3 at the Zhangye site from 17 April 17 to 18 June 2008.

ticles for the TEOM, 91% for 5 μm particles for the nephelometer, and 75% for 5 μm particles for the Aethalometer. The penetration efficiencies for particles smaller than 2.5 μm are all greater than 95%.

2.4. Meteorology

[17] A Vaisala Model WXT-510 (Helsinki, Finland) weather transmitter, mounted on top of the COMMIT trailer ~4 m above the surface, logged ambient temperature, relative humidity, ambient pressure, wind speed, and wind direction every minute. Five minute and hourly averages were used in this study.

2.5. Emission Inventory

[18] The anthropogenic emissions of CO, SO_2, and NO_x in 2006 were estimated by *Zhang et al.* [2009] for Asian countries. The emission rates of 0.5° × 0.5° resolution were allocated into grid cells of 27 km × 27 km, using population and road network density as surrogates [*Du*, 2008; *Fu et al.*, 2009]. Emissions in each cell from four sectors (power, industry, transportation, and residential) were further distributed into 12 vertical layers: layer 1 including the transportation and domestic sectors represents the area and mobile sources near the surface; layer 2 accounts for small power plants and industrial emissions; layer 3 and above contain emissions from large point sources. We did not extrapolate the estimated emissions for 2006 to 2008, the year of our experiment, as the focus of this study is on the characteristics of local emission sources. The total pollutant emissions from this rural area could grow significantly in two years, but the properties of different emission sectors (e.g., the CO/SO_2 emission ratio for industrial and residential sources) are not expected to change as dramatically. In other words, there could be more factories in the area in 2008 than in 2006, but we assume that the technology and emission characteristics remain largely unchanged.

3. Analysis and Discussion

3.1. Levels of Trace Gases and Aerosols

[19] The time series plots of NO, NO_y^*, SO_2, CO, and O_3 at the Zhangye site are given in Figure 2 to illustrate the levels and variability of trace gases during the experiment. Statistics of gases and aerosols are summarized in Table 1. The concentrations of NO_y^* (4.2 ± 3.4 ppb, hereafter results given as mean ± standard deviation of hourly averaged data), SO_2 (3.4 ± 4.8 ppb), and CO (265 ± 161 ppb) are considerably lower than those observed in eastern China. For example, at rural sites near Shanghai [*Wang et al.*, 2004] and Beijing [*C. Li et al.*, 2007], the springtime levels of NO_y, SO_2, and CO were found to be 13.8–26.0 ppb, 15.9–17.8 ppb, and 680–1090 ppb, respectively. The maxima of NO_y^*, SO_2, and CO in Zhangye, on the other hand, were substantial at 23.1 ppb, 40.3 ppb, and 1287 ppb, implying the influences of local and regional anthropogenic emissions. In Lanzhou, another city in the Hexi Corridor and about 450 km to the southeast, the SO_2 levels in April were about 0.5 mg/m^3 or ~200 ppb [*Chu et al.*, 2008]. During our experiment in Zhangye, O_3, a product of photochemical reactions in the atmosphere, was 48.5 ± 15.4 ppb with an hourly maximum of 83.0 ppb, suggesting moderate photochemical processes. Much of the temporal variation in the trace gases was controlled by the

Table 1. Statistics of Trace Gases and Aerosol Properties During the Experiment[a]

	Mean	Standard Deviation	Median	10th Percentile	25th Percentile	75th Percentile	90th Percentile
CO (ppb)	265	161	201	141	159	313	474
NO (ppb)	0.41	0.60	0.17	0.03	0.07	0.45	1.1
NO_y^* (ppb)	4.2	3.4	3.3	0.8	1.7	5.8	8.8
SO_2 (ppb)	3.4	4.8	1.6	0.3	0.7	4.1	8.7
O_3 (ppb)	48.5	15.4	51.4	25.5	37.2	60.2	66.0
B_{sp} (Mm^{-1})	159	191	105	41	63	196	293
B_{ap} (Mm^{-1})	10.3	9.1	7.0	2.5	4.0	13.7	23.4
PM_{10} ($\mu g/m^3$)	153	230	95	45	63	160	264

[a]All aerosol data reported for volumes under 1013.25 hPa and 20°C.

diurnal change in meteorological conditions, as discussed in section 3.2.

[20] Aerosol loadings during the Zhangye experiment were high and variable, likely a result of strong and episodic dust emissions in the region (Figure 3). The hourly PM_{10} was 153 ± 230 $\mu g/m^3$, comparable to the 145 $\mu g/m^3$ mean level observed in a rural location near Beijing from January to March [*Chaudhry et al.*, 2007]. A spring field campaign around a sandy area, north of Beijing, found average PM_{10} levels between 226 and 522 $\mu g/m^3$ [*Cheng et al.*, 2005]. Some thirty aerosol samples collected in Dunhuang, 500 km to the northwest of Zhangye, yielded an average TSP (total suspended particulate) concentration of 317 $\mu g/m^3$ in spring 2001 [*Zhang et al.*, 2003b]. The average PM_{10} was 158 $\mu g/m^3$ during an almost yearlong experiment in Dunhuang 3 years later [*Yan*, 2007].

[21] For this experiment, the hourly aerosol scattering coefficient (B_{sp}) at 500 nm was 159 ± 191 Mm^{-1}. The large standard deviations in PM_{10} and B_{sp} data are likely due to episodic strong dust events. The aerosol absorption coefficient (B_{ap}, 500 nm) was less variable, averaged at 10.3 ± 9.1 Mm^{-1}, with a maximum of 61.1 Mm^{-1}. The comparison between different studies can be complicated, particularly for measurements of aerosol absorption and instruments with different size cut. However, it may still be meaningful considering that fine particles ($PM_{2.5}$ or smaller) likely dominate aerosol extinction in most cases. In Dunhuang B_{sp} was ~150 Mm^{-1} from April to June in 2004 [*Yan*, 2007]. At another desert site in Yulin, roughly midway in between Beijing and Zhangye, *Xu et al.* [2004] noted that B_{sp} was 158 ± 193 Mm^{-1}, to go along with a B_{ap} of 6 ± 11 Mm^{-1}, for $PM_{2.5}$ in April. B_{sp} and B_{ap} values obtained from eastern China were generally greater: B_{sp} of 353 Mm^{-1} and B_{ap} of 23 Mm^{-1} for $PM_{2.5}$ were logged in a rural location around Shanghai [*Xu et al.*, 2002]; similarly high B_{sp} (468 Mm^{-1}) and B_{ap} (65 Mm^{-1}) for bulk aerosols were recorded near Beijing [*C. Li et al.*, 2007]. A recent study coordinating observations at 14 locations in China [*Zhang et al.*, 2008] also suggested stronger aerosol absorption in urban and suburban areas in eastern China.

[22] Several dust events, including three intense ones in early May (2–3, 8–9, and 11 May, or DOY 123–124, 129–130, and 132), stand out in the time series of PM_{10}, B_{sp}, and aerosol size distribution (Figures 3a, 3c, and 3d). During these dust storms, the hourly PM_{10} reached well above 1000 $\mu g/m^3$, and B_{sp} could exceed 1000 Mm^{-1}. Meanwhile the peak in the aerosol number size distribution shifted from submicron to supermicron particles. The aerosol absorption coefficient, on the other hand, showed much smaller increases. The light absorption of dust particles at around 500 nm appears to be small compared to anthropogenic pollutants, as also suggested by previous studies near the dust source regions in China [e.g., *Cheng et al.*, 2006; *Xia et al.*, 2005; *Xu et al.*, 2004].

3.2. Diurnal Variations

[23] A regular diurnal wind pattern was observed during the experiment (Figure 4): strong northwest wind prevailed in the daytime, from 1100 to 1900 LT (local time), followed by weak and variable wind mainly from south during 2000–2300 LT, and then southeasterly gradually gaining strength from midnight until 0900 LT the next morning, when northwest wind started to take over again. This phenomenon is probably explained by the valley terrain of the area. During daytime, solar heating of the northern slope of the Qilian Mountains warms up the air above, inducing upslope northerly wind, or the valley wind, which generally peaks near midday and dies down before sunset. At night, the radiative cooling of the mountain slope cools down the layer of air in contact with it. The cooler airflows northward down the slope, forming the mountain wind, which usually reaches maximum strength just before sunrise [*Arya*, 1999]. For this arid area temperature showed a large diurnal range and RH often remained below 50% all day (Figure 4).

[24] Closely related to the local meteorology, trace gases and aerosols also demonstrated pronounced diurnal features (Figure 4). Afternoon levels of primary pollutant gases were almost always low, with CO of ~150 ± 20 ppb, SO_2 of ~1.1 ± 1.0 ppb, and NO_y^* of ~2.0 ± 2.0 ppb. This is unlike the eastern United States, where SO_2 maxima are normally observed during daytime when vertical mixing brings emissions from upwind point sources to near the surface [e.g., *Stehr et al.*, 2000]. The afternoon CO concentration is close to the lower free tropospheric level measured at Mount Waliguan, a nearby background site (36.29°N, 100.90°E, 3810 m above sea level, NOAA/GMD, webpage: http://www.esrl.noaa.gov/gmd/ccgg/iadv/), suggesting generally small influences of local anthropogenic pollution. Strong northwesterly wind from the Gobi deserts and vigorous daytime vertical mixing efficiently dissipate pollutants from the local sources. Light wind and suppressed vertical motion at night favor the accumulation of pollutants near the surface, and nighttime concentrations were generally greater (Figure 4). The maxima of CO (414 ± 164 ppb), SO_2 (8.1 ± 6.5 ppb), and NO_y^* (7.3 ± 6.7 ppb) appeared at around 0800 LT, after hours of southeast wind carrying pollutants from the Zhangye city and the surrounding areas to the site. Increased human activities (more traffic and starting of business) and the downward mixing of emissions from small point sources (e.g., nearby factories) in the early morning may also contribute to the morning peaks in

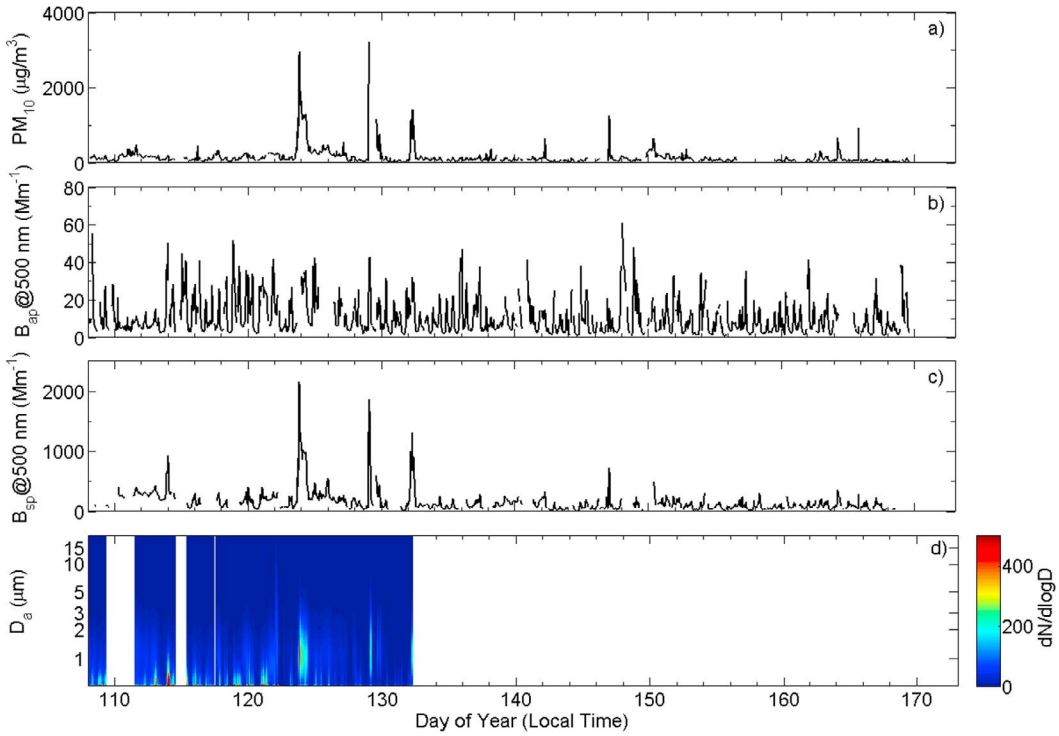

Figure 3. Same as Figure 2 but for (a) PM_{10}, (b) aerosol absorption coefficient at 500 nm, (c) aerosol scattering coefficient at 500 nm, and (d) aerosol size distribution (unit: cm^{-3}).

the primary pollutants. Smaller CO and NO_y^* peaks with little SO_2 appearing at 2000–2300 LT likely reflect a mixture of sources near the surface. Emissions of mobile sources and biofuel combustion normally containing CO and NO_x but little SO_2 could be brought to the site, by southerly wind from the major highway and villages. In section 3.3, we further discuss the influences and characteristics of local emission sources. Unlike the primary gases, O_3 had the maximum (63.5 ± 7.0 ppb) in the afternoon (Figure 4) when the photochemical processes are most active. The broad peak during daytime (1000–1800 LT), and the fast increase in the morning (0600–1000 LT) imply that the downward mixing from the residual layer might also be an important source of surface O_3. Removed through dry deposition and gas titration, O_3 reached its daily low (29.6 ± 12.8 ppb) just before dawn. The mountain wind prevented the formation of a very stable nocturnal boundary layer and O_3 seldom dropped below 10 ppb.

[25] The diurnal variation in aerosol absorption coefficient (B_{ap}) was well synchronized with CO (Figure 4). Two comparable peaks of B_{ap} appearing at 0800 LT (17.8 ± 12.0 Mm^{-1}) and 2100 LT (18.9 ± 13.2 Mm^{-1}) were likely associated with anthropogenic emissions. The low in B_{ap} (3.5 ± 1.8 Mm^{-1}), a factor of 5 smaller than the maxima, was found at 1400 UTC when the influence of pollution was minimal. Aerosols (number concentration) comprising mainly submicron particles at night (Figure 4) were characteristic of anthropogenic emissions, although the number of supermicron particles was still substantial. With strong wind from the desert and possible local dust emissions, aerosols in the afternoon were dominated by supermicron particles, presumably dust (Figure 4). The diurnal cycles of PM_{10} and aerosol scattering (B_{sp}) were generally in phase with that of B_{ap} but not as large. The daily maxima of aerosol mass (209 ± 463 $\mu g/m^3$) and scattering (228 ± 307 Mm^{-1}) were found at 0100 LT, probably skewed by the few dust storms mentioned earlier. Slightly smaller peaks in PM_{10} (morning: 194 ± 240 $\mu g/m^3$; evening: 200 ± 413 $\mu g/m^3$) and B_{sp} (morning: 202 ± 230 Mm^{-1}; evening: 187 ± 294 Mm^{-1}) in the morning and evening hours roughly doubled the daily lows in the afternoon (PM_{10}: 101 ± 80 $\mu g/m^3$; B_{sp}: 92 ± 72 Mm^{-1}). Dust particles were likely present in the area throughout a day, responsible for a large fraction of PM_{10} and B_{sp} but a relatively small fraction of B_{ap}. The latter mainly controlled by anthropogenic emissions thus demonstrated a more marked diurnal variation.

[26] Under the assumption that the shortwave light extinction is completely due to particles with diameters of 10 μm or less, we estimate the mass scattering efficiency for PM_{10} aerosols at ~0.9 m^2/g in the afternoon and ~1.0 m^2/g in the morning, comparable to the 1.05 m^2/g observed in Dunhuang in spring [*Yan*, 2007]. The mass scattering efficiencies determined for $PM_{2.5}$ aerosols in Yulin were 3.0 m^2/g for pollution and 1.0 m^2/g for dust [*Xu et al.*, 2004]. Likewise, the mass absorption efficiency in the dust-dominant afternoon was only ~0.03 m^2/g, compared to the morning value of ~0.1 m^2/g for the dust-pollution mixture. Our observed diurnal change in the mass extinction efficiency likely mirrors the change in aerosol composition. The single scattering albedo (SSA, at 500 nm), defined as the ratio between aerosol scattering and extinction (scattering + absorption), also showed distinct difference between day and night (Figure 4). The peak SSA values (0.95 ± 0.02) for dust dominant particles in the afternoon were close to another field experiment

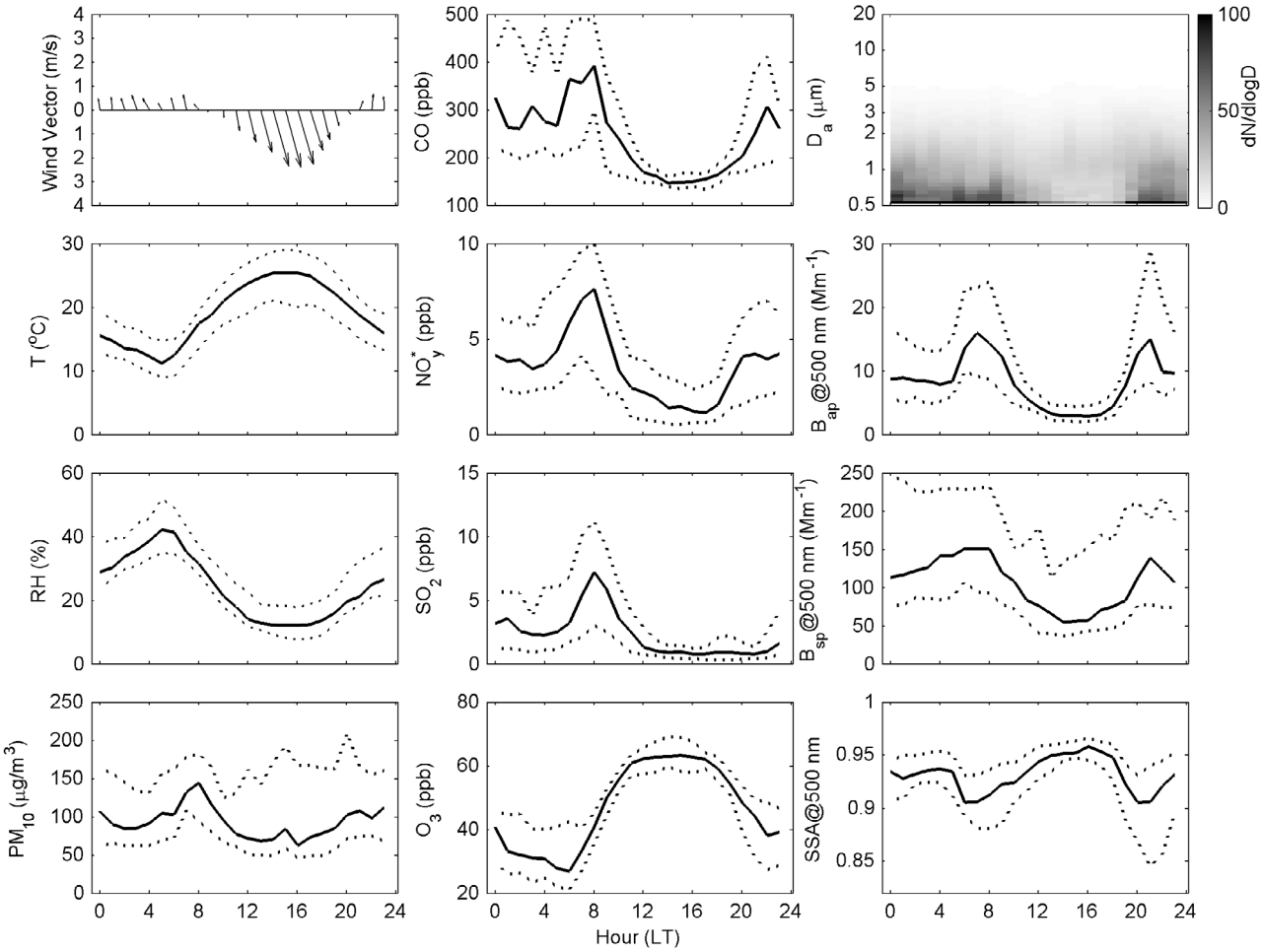

Figure 4. The diurnal variations in (first row, left to right) wind, CO, aerosol size distribution, (second row, from left to right) temperature, NO_y^*, aerosol absorption coefficient, (third row, from left to right) relative humidity, SO_2, aerosol scattering coefficient, (fourth row, from left to right) PM_{10} level, O_3, and aerosol single scattering albedo in Zhangye from 17 April to 18 June 2008 (17 April to 11 May for aerosol size distribution). Median values (solid lines) are shown to give a more distinct diurnal pattern than means, which could be influenced by a few extreme dust events. The dotted lines are the 25th (lower) and 75th (upper) percentiles for each hour of the day. The unit for aerosol size distribution is cm^{-3}.

(0.95 ± 0.05 [*Xu et al.*, 2004]) and several remote sensing studies investigating the airborne dust in northern China [e.g., *Cheng et al.*, 2006; *Lee et al.*, 2007; *Xia et al.*, 2005]. The daily low SSA (0.89–0.91) in Zhangye was still greater than in both urban (0.81 [*Bergin et al.*, 2001]) and rural areas (0.81–0.85 [*C. Li et al.*, 2007]) close to Beijing, probably due to dust particles at night. Another study conducted near Beijing by *Yan et al.* [2008] gave SSA of 0.88, but their data spanned over a year, including summer when aerosol scattering may be enhanced by hygroscopic growth and secondary aerosols.

[27] The wind roses in Figure 5 provide some further insights into the connection between meteorology and pollution. With wind mainly from southeast and wind speed over 4 m/s most of the time, morning (0600–0900 LT, Figure 5a) measurements probably represent emissions from both local sources and a relatively large area along the valley. Under more stagnant conditions, measurements in the evening hours (2000–2300 LT, Figure 5b) may be largely influenced by local emission sources. Consistent with Figure 4, NO_y^* (Figure 5c), SO_2 (Figure 5d), and CO (Figure 5e) during the whole experiment were in general more abundant in southeast wind. PM_{10} (Figure 5f) and B_{sp} (Figure 5g) did not show a strong dependence on wind direction. Northwest wind may bring dust while southeast wind may transport pollutants. B_{ap}, on the other hand, was greater in southeast wind and more closely associated with anthropogenic emissions.

3.3. Characteristics of the Local Anthropogenic Emission Sources

[28] This experiment lends us a good opportunity to characterize the anthropogenic emission sources in a region that so far has been understudied. The diverse local emission sources near the site, on the other hand, can impact our measurements, as revealed in Figure 6, which shows simultaneous 5 min data of CO and SO_2. The spread of the data points reflects a variety of source types encountered during the experiment. The upper edge with high CO/SO_2 ratio probably represents less efficient combustion sources near the surface such as domestic emissions, whereas the lower edge

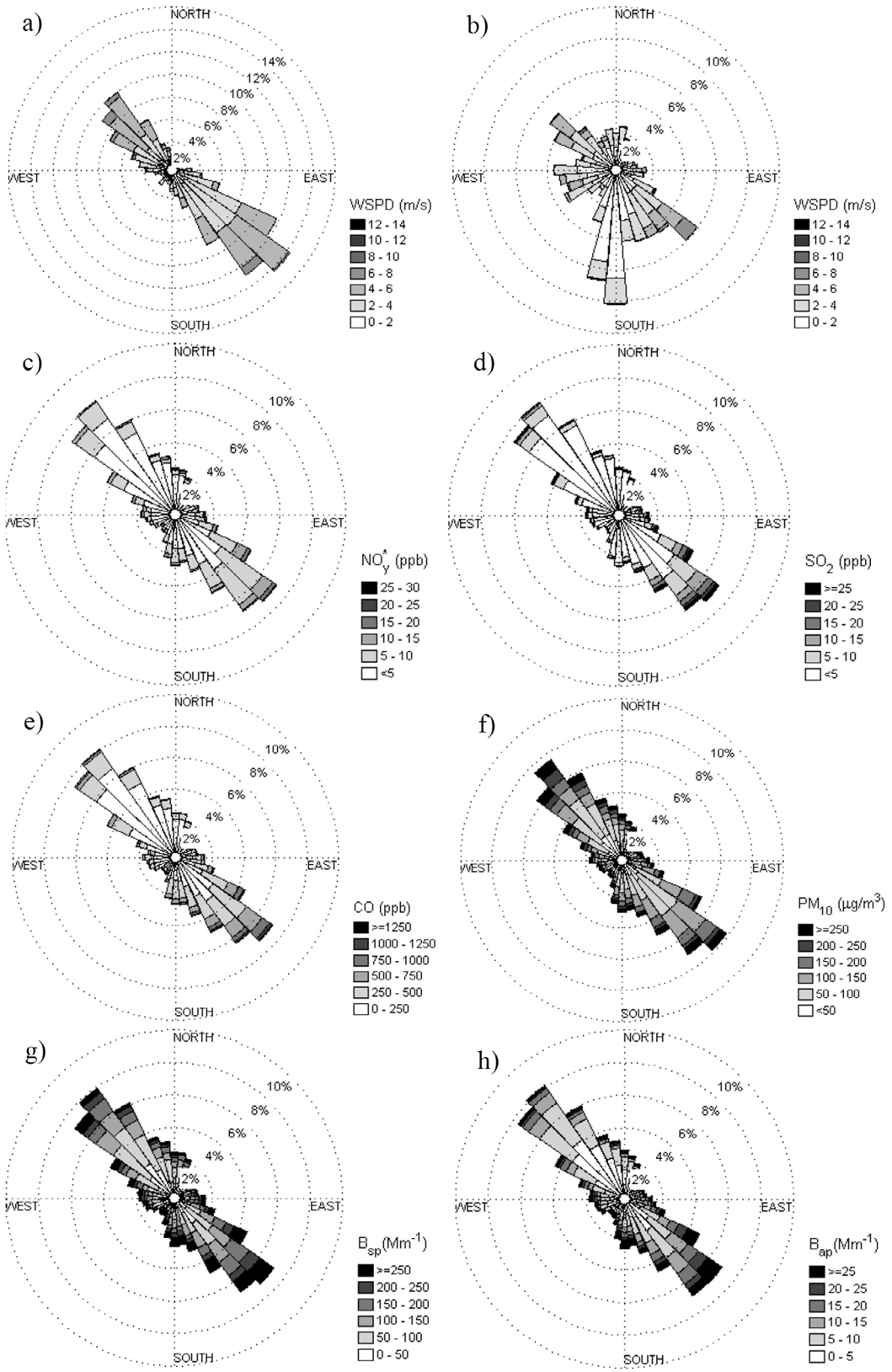

Figure 5. Wind roses for (a) morning (0600–0900 LT) and (b) evening (2000–2300 LT) hours; shade represents wind speed. Wind roses for all hours, with shade representing levels of (c) NO_y^*, (d) SO_2, (e) CO, (f) PM_{10}, (g) aerosol scattering coefficient, and (h) aerosol absorption coefficient. Date during strong dust episodes are excluded in Figures 5c–5h.

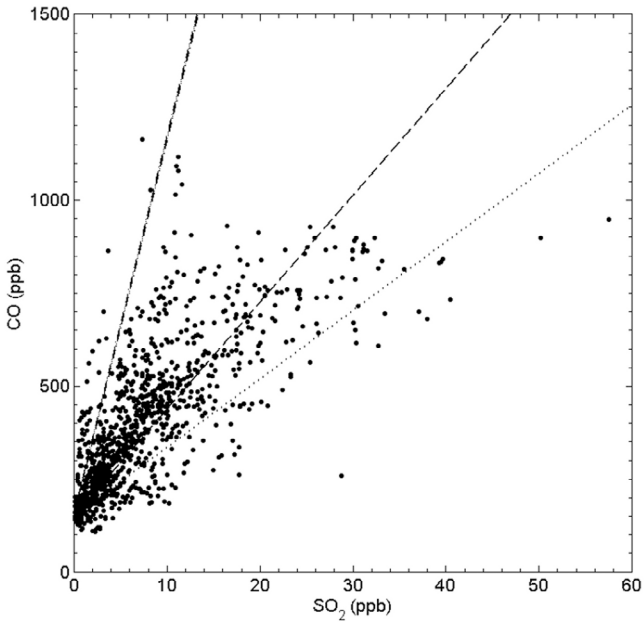

Figure 6. The scatterplot of 5 min CO-SO_2 data in morning hours (0600–0900 LT) excluding the dust storms. The dash-dotted line stands for the 2006 INTEX-B inventory [*Zhang et al.*, 2009] emission ratios between the corresponding gases for Layer 1 (residential and transportation sectors) sources within ~100 km from the site. The dotted and dashed lines represent the inventory ratios for layer 2 (industry and power sectors) and all (layers 1 and 2) sources, respectively. An intercept of 150 ppb CO was assumed for the CO/SO_2 inventory ratios to account for the daytime background CO level.

having relatively low CO/SO_2 may reflect more efficient coal burning from nearby small point sources, for example, boilers in factories. The inventory CO/SO_2 emission ratios are also given in Figure 6, for layer 1 (residential and transportation; see section 2.5), layer 2 (small power plants and industry), and all (layers 1 and 2) sources within ~100 km from the site, as estimated in the 2006 Intercontinental Chemical Transport Experiment−Phase B (INTEX-B) emission inventory [*Zhang et al.*, 2009]. The measured CO/SO_2 ratio seems to be in reasonable agreement with the inventory, as the majority of the paired measurements are bounded by the layer 1 and 2 inventory ratios.

[29] The influence of local emission sources can also be identified as spikes in the 5 min time series plots. We looked for these local pollutant peaks in CO, SO_2, NO_y^*, and B_{ap} that satisfy the thresholds in amplitude (peak height) and sharpness (to avoid broad peaks). The choice of the threshold values was somewhat subjective, but could be adjusted to achieve the inclusion of the most prominent peaks and the exclusion of small features. After some iteration, ~60–90 spikes picked out for each pollutant were further examined. Only those observed under relatively stable wind direction and showing maxima for at least two species were retained for additional analysis.

[30] A number of the identified pollutant peaks appeared between ~0700 and ~1100 LT, coincident with the onset of more vigorous vertical mixing in the atmosphere during daytime. As shown in the example in Figure 7, substantial SO_2 and NO were observed along with these spikes, suggesting that they were fresh plumes originating from nearby coal-burning sources, such as small industrial boilers. Our estimated NO_x/NO_y^* ratio for these plumes is generally >0.6, and the NO_y^* concentration can be used to derive NO_y level with relatively small uncertainty (typically <30%). Assuming that these pollutant peaks reflect emissions from nearby sources superimposed on a more slowly evolving regional background, we can try to estimate both the background and the local contributions. The regional background concentrations were inferred by linearly interpolating measurements before and after the peak (see dotted lines in Figure 7). The determined background depends on the perception of the start and the end of a particular peak, but the uncertainty should be small for more distinct spikes. The contributions from the local sources to different species, ΔCO, ΔSO_2, ΔNO_y, and ΔBC, were then estimated as the difference between the inferred background and the ambient levels. The ratios for $\Delta CO/\Delta SO_2$, $\Delta CO/\Delta NO_y$, $\Delta NO_y/\Delta SO_2$, and $\Delta BC/\Delta CO$ for each plume, obtained through linear correlation analysis as illustrated in Figure 8, should reflect the emission characteristics of the corresponding local sources. Table 2 summarizes the ratios derived from the morning pollutant spikes. Only results with R^2 (correlation coefficient) ≥0.5 are included. We focus on results based on NO_y values estimated using method 1 (see section 2.2). The ratios derived using methods 1 and 2 differ by less than 5% when both are available.

[31] The $\Delta CO/\Delta SO_2$ ratio (by moles) of the morning pollutant peaks ranges from 24.6 to 54.2, and the average industrial emission ratio estimated by *Zhang et al.* [2009] is 71.9 for the grid cell in which our site was located (39°N–39.5°N, 110°E–110.5°E), and 43.7 for the larger area (38°N–40°N, 99°E–101.5°E). The $\Delta CO/\Delta NO_y$ ratio has a small range between 25.8 and 35.9, greater than the emission inventory for the industry sector (25.7 and 23.7 for the local cell and the larger area, respectively). The $\Delta NO_y/\Delta SO_2$ ratio from the measurements at 0.79–1.52 compares lower than the industrial inventory ratios of 2.79 (local cell) and 1.84 (large area). The $\Delta NO_y/\Delta SO_2$ ratio near unity is likely a result of low-tech combustion of high sulfur coal. The BC/CO emission ratio (by mass) for the industry is estimated at 3.4–4.0 × 10^{-3} (local cell and the larger area) in the emission inventory [*Zhang et al.*, 2009], compared to 4.1–6.1 × 10^{-3} for the morning peaks. The differences in CO/NO_y and NO_y/SO_2 ratios between the inventory and measurements point to a possible overestimate of NO_x emissions. There is however uncertainty associated with both measurements and emission inventory. Below we discuss the limitations of using our results to evaluate the inventory.

[32] As mentioned above, the analysis of individual plumes is subject to uncertainty in the inferred background concentration. We can further examine the fresh plumes in the early morning (0600–0900 LT), by selecting all the data with $NO_x/NO_y^* > 0.7$, and NO > 0.2 ppb. A correlation analysis of these data points yields a CO/NO_y ratio of 30 (Figure 9), and an intercept (116 ppb CO) close to the minimum CO level observed during daytime. The CO/NO_y ratio is consistent with the $\Delta CO/\Delta NO_y$ ratio from the individual plumes, suggesting the robustness of the analysis. As another sensitivity test, we estimate the pollutant ratios for the morning

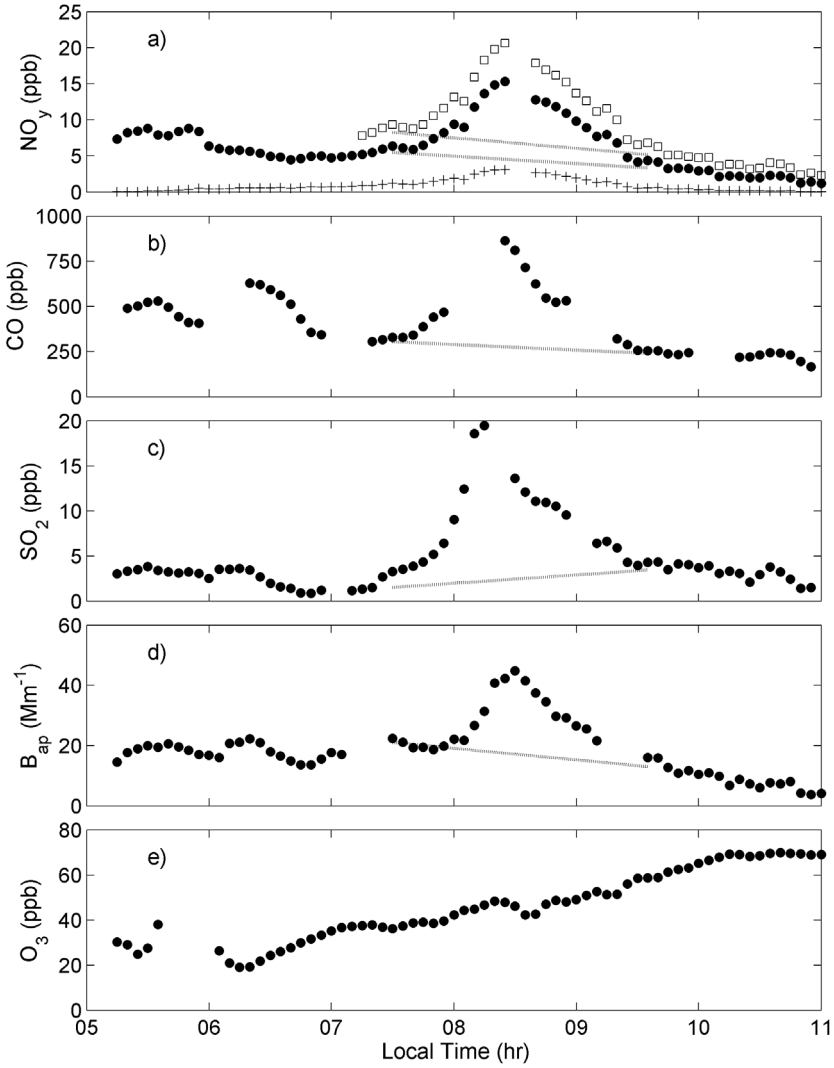

Figure 7. Time series of (a) NO_y (pluses, NO; solid circles, NO_y^*), (b) CO, (c) SO_2, (d) aerosol absorption coefficient, and (e) O_3 during a local pollution plume observed in the morning of 27 April 2008. Dotted lines are the baselines of NO_y/NO_y^*, CO, and SO_2, and aerosol absorption, inferred by linearly interpolating the concentrations before and after the peak of the plume. Wind was from ESE during the plume before turning to N at ~0900 LT.

plume peaks (Table 2) assuming fixed background levels (10th percentiles in Table 1, i.e., 141 ppb CO, 0.3 ppb SO_2, 0.8 ppb NO_y^*, and 2.5 Mm^{-1} B_{ap}). This results in generally consistent ranges of $\Delta CO/\Delta SO_2$ (25.8–52.3 versus 24.6–54.2), $\Delta CO/\Delta NO_y^*$ (21.3–44.2 versus 25.8–35.9), $\Delta NO_y^*/\Delta SO_2$ (0.72–2.3 versus 0.79–1.31), and $\Delta BC/\Delta CO$ (4.0–7.8 × 10^{-3} versus 4.1–6.1 × 10^{-3}), compared to the previous method using background derived from measurements before and after a local plume. The ratios derived for some individual plumes can be significantly influenced by the selected background, particularly for those superimposed on heavy regional pollution, but the ranges of the ratios from all plumes are relatively insensitive.

[33] Besides the assumed background, our estimated ranges may also reflect one or more of the following factors: the sampling of the plumes for the analysis, changes in meteorology and transport, and the actual variations in emissions. Given the relatively small sample size, the derived pollutant ratios are uncertain and need be interpreted with caution. Most of the selected plumes are captured under prevailing southerly winds in the morning, and this may lead to a mismatch between our sampled plumes and the actual emission sources nearby. For comparison, the emission inventory is of coarse resolution and incorporates different industrial sources. Additional analysis involving numerical simulation of meteorological conditions and pollutant transport, in addition to more extensive measurements of ambient pollutants and emission sources, may be necessary before the emission inventory for the region can be evaluated with more confidence.

[34] Results from similar analysis on nighttime pollutant peaks are given in Table 3. As discussed in section 3.2, the O_3 concentration was well above zero and NO remained low at night (mostly below 80 ppt), even for local peaks with elevated NO_y^* levels. ΔNO_y^* estimated for these peaks, however, may still be regarded as a close lower limit for ΔNO_y, as it

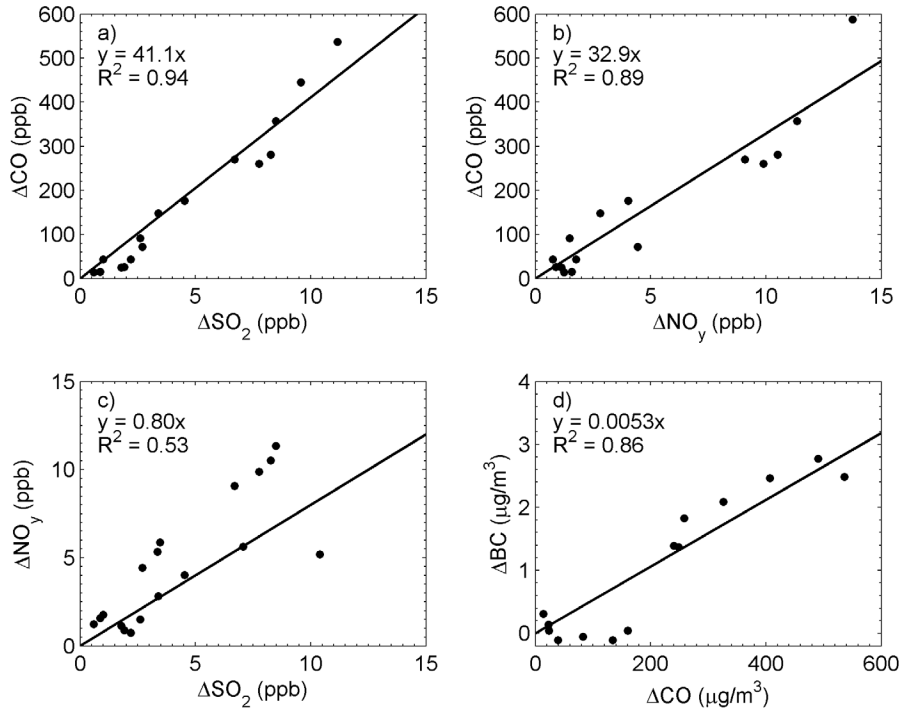

Figure 8. Scatterplots of (a) ΔCO-ΔSO_2, (b) ΔCO-ΔNO_y, (c) ΔNO_y-ΔSO_2, and (d) ΔBC-ΔCO for the local pollution plume shown in Figure 7. ΔCO, ΔSO_2, ΔNO_y, and ΔBC were derived as the difference between the ambient and the inferred background (dotted lines in Figure 7) concentrations. The solid lines represent the results of linear correlation analysis, with intercepts forced to be zero. B_{ap} data were converted into the black carbon (BC) concentration, assuming a mass absorption efficiency of 10 m^2/g. Mass concentration of CO was calculated using simultaneously measured pressure and temperature.

probably represents contributions from nearby sources that have experienced limited chemical aging at night. Local minima in O_3 were also recorded for the majority of these nighttime spikes, further evidence that the plumes were relatively fresh. As expected, a variety of emissions sources were captured at night, with $\Delta CO/\Delta SO_2$ (10.4–116.7), $\Delta CO/\Delta NO_y^*$ (21.5–155.9), $\Delta NO_y^*/\Delta SO_2$ (0.12–2.29), and $\Delta BC/\Delta CO$ (2.4–12 × 10^{-3}) ratios all having wide ranges. In comparison, the CO/NO_x inventory emission ratio for the area can be over 100 for the residential sector, and less than 15 for the transportation sources, while the CO/SO_2 inventory ratio for the same two sectors is near or over 100 [*Zhang et al.*, 2009]. The inventory NO_x/SO_2 ratio is more than 60 for traffic emissions and 0.8–0.9 for residential sources. The BC/CO inventory ratio for these two sectors in the area is 7–20 × 10^{-3} [*Zhang et al.*, 2009]. Both measurements and the emission inventory at least partly reveal the diverse nature of emission sources in the region.

3.4. Mixing of Dust and Anthropogenic Pollutants Near the Dust Source Region

[35] As discussed in section 3.2, the mixing between dust particles and anthropogenic pollutants likely occurred regularly at night, when anthropogenic emissions accumulated near the surface. On the other hand, strong episodic dust storms tend to carry dust into large downwind areas. These dust storms are often associated with synoptic or mesoscale

Table 2. Results of Correlation Analysis for Local Pollutant Peaks Observed in the Morning[a]

Day of Year (LT)	$\Delta CO/\Delta SO_2$[b]	R^2	$\Delta CO/\Delta NO_x$[b]	R^2	$\Delta NO_x/\Delta SO_2$[b]	R^2	$\Delta BC/\Delta CO$[c]	R^2	Wind direction
114.32–114.44					1.10[d]	0.94			SE
116.26–116.39	27.7	0.85	33.6[e]	0.72	0.79[e]	0.51	5.5 × 10^{-3}	0.78	SE
118.31–118.40	41.1	0.94	32.9	0.89	0.80	0.53	5.3 × 10^{-3}	0.86	ESE
119.26–119.38	24.6	0.83							SE
126.41–126.49					0.81	0.93	5.5 × 10^{-3}	0.64	N
130.28–130.36	54.2	0.74					6.1 × 10^{-3}	0.88	SE
143.30–143.39	39.7	0.76	25.8	0.65	1.52	0.83	4.2 × 10^{-3}	0.82	SE
167.34–167.39	46.8	0.94	35.9[d]	0.95	1.31[d]	0.99	4.1 × 10^{-3}	0.69	NW

[a]Only results with $R^2 \geq 0.5$ are included.
[b]Unit is ppb/ppb.
[c]Unit is ($\mu g/m^3$)/($\mu g/m^3$).
[d]The $j(NO_2)$ value were calculated using equation (2) used for NO_y data.
[e]$NO_x/NO_y^* > 0.9$; no correction was made.

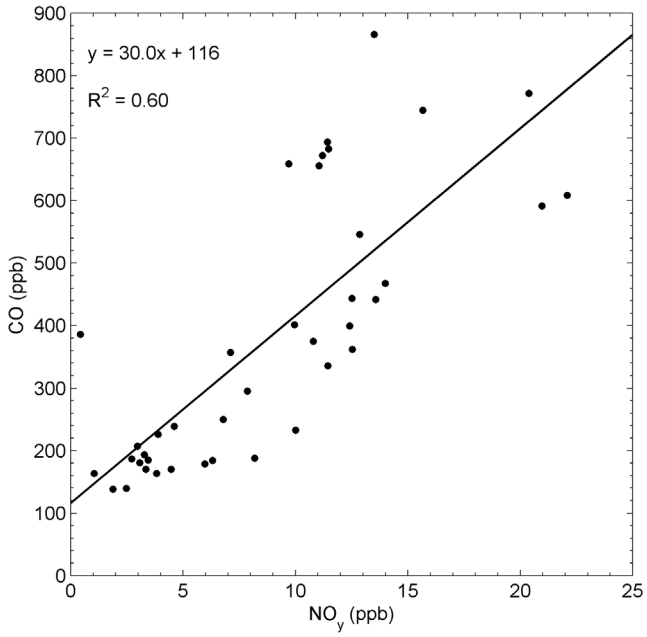

Figure 9. Scatterplot of CO and NO_y for 5 min morning (0600–0900 LT) data points with $NO_x/NO_y^* > 0.7$ and NO > 0.2 ppb. The solid line represents the result of linear correlation analysis.

disturbance, which would also influence the ambient levels of pollutants.

[36] On the evening of 2 May (DOY 123), a severe dust storm was brought to the Zhangye site by strong northerly wind (Figure 10, 1400–2100 LT). At its peak (1700–2100 LT), the dust storm possessed 5 min PM_{10} level around 4000 $\mu g/m^3$ (Figure 10a), and the CO and SO_2 concentrations (Figures 10b and 10c) near the low daytime levels. The O_3 concentration (Figure 10d) stayed relatively high at ~60 ppb well into the night, as strong wind dissipating near surface emissions slowed O_3 titration. The aerosol single scattering albedo for the dust was about 0.98 (Figure 10e), similar to that measured for "clean" Asian dust particles [*Anderson et al.*, 2003]. The aerosol size distribution was dominated by particles of 1–2 μm in aerodynamic diameter (Figure 10g).

[37] By midnight the strong northerly wind had diminished and been replaced by weaker southerly wind, but dust particles remained in the air, as evidenced by PM_{10} of ~2000 $\mu g/m^3$ (Figure 10a) and the abundant supermicron particles (Figure 10h). Under lower wind speed, a well-defined CO peak of almost 1000 ppb appeared between 0300 and 0600 LT (Figure 10b), as did SO_2 of up to 8 ppb (Figure 10c). The NO_y^* concentration (not shown) also increased by about 2 ppb, but did not show a peak as evident. Good correlation between CO and SO_2 ($R^2 = 0.54$) and the CO/SO_2 ratio of about 78 (intercept: 303 ppb) implied that the gases were from residential sources. If calcite ($CaCO_3$) makes up 10% of the dust and has a concentration of ~1 $\mu mol/m^3$, the peak SO_2 of ~0.2–0.3 $\mu mol/m^3$ is enough to neutralize 20–30% of the calcite, provided there is complete conversion to H_2SO_4. The decrease in O_3 concentration at the same time was likely due to gas-phase titration, also suggesting the accumulation of pollutants near the surface. Accompanying the CO and SO_2 peaks was a dip in SSA from 0.98 to 0.95 (Figure 10e), possibly due to BC from the same emission sources. The aerosols in the trace gas plume, although still mainly consisting of supermicron particles, also saw a substantial increase in submicron particles (Figure 10h). While the data set from this dust episode provided little evidence of the processing of trace gases (SO_2 and NO_y^*) by dust particles, it clearly showed that the anthropogenic aerosols can mix with dust over its source region, modifying the bulk optical properties and size distribution of aerosols. The dust event extended well after the gas plume disappeared (Figure 10a). The observed mixing between dust and anthropogenic pollutants in the area occurred in relatively weak southerly wind, after strong northerly wind had died down. During daytime on 3 May, convective processes may facilitate the upward transport of dust particles, and relatively strong northwesterly winds (up to 6 m/s on the ground, not shown) could transport the dust aerosols mixed with anthropogenic pollutants to other areas. Furthermore, anthropogenic pollutants emitted at the night of 2 May, during the peak of the dust storm, although not detected due to strong ventilation by the northerly wind, likely would still mix with dust particles and can accompany the dust plume to downwind areas.

[38] Meteorological records and lidar measurements at different locations [*Z. Huang et al.*, 2010] on 2 May indicated that this dust event may spread over other locations within the

Table 3. Results of Correlation Analysis for Local Pollutant Peaks Observed at Night[a]

Day of Year (LT)	$\Delta CO/\Delta SO_2$[b]	R^2	$\Delta CO/\Delta NO_x^*$[b]	R^2	$\Delta NO_x^*/\Delta SO_2$[b]	R^2	$\Delta BC/\Delta CO$[c]	R^2	Wind Direction
116.96–117.02	10.4	0.93	41.6	0.89	0.24	0.97	3.4×10^{-3}	0.82	NW
117.79–117.86	22.6	0.89	102.5	0.93	0.22	0.84	5.5×10^{-3}	0.92	NW
118.97–119.04					0.12	0.56	2.6×10^{-3}	0.75	SE
120.91–120.99			32.5	0.64					SE
123.04–123.16	40.7	0.78	155.9	0.84			2.4×10^{-3}	0.83	SE
125.96–126.02	116.7	0.81	75.6	0.84	1.54	0.93			SE
126.77–126.85	73.7	0.84	62.3	0.61			1.2×10^{-2}	0.67	N
149.01–149.11	14.7	0.78							SE
152.04–152.11	23.8	0.83	81.4	0.74					E
157.83–157.94			101.0	0.66					NW
160.09–160.14	49.2	0.95	21.5	0.98	2.29	0.96	6.3×10^{-3}	0.79	NW
161.94–162.04	45.7	0.82	97.0	0.92					NW
164.91–165.01	34.2	0.64							NW

[a]Only results with $R^2 \geq 0.5$ are included.
[b]Unit is ppb/ppb.
[c]Unit is ($\mu g/m^3$)/($\mu g/m^3$).

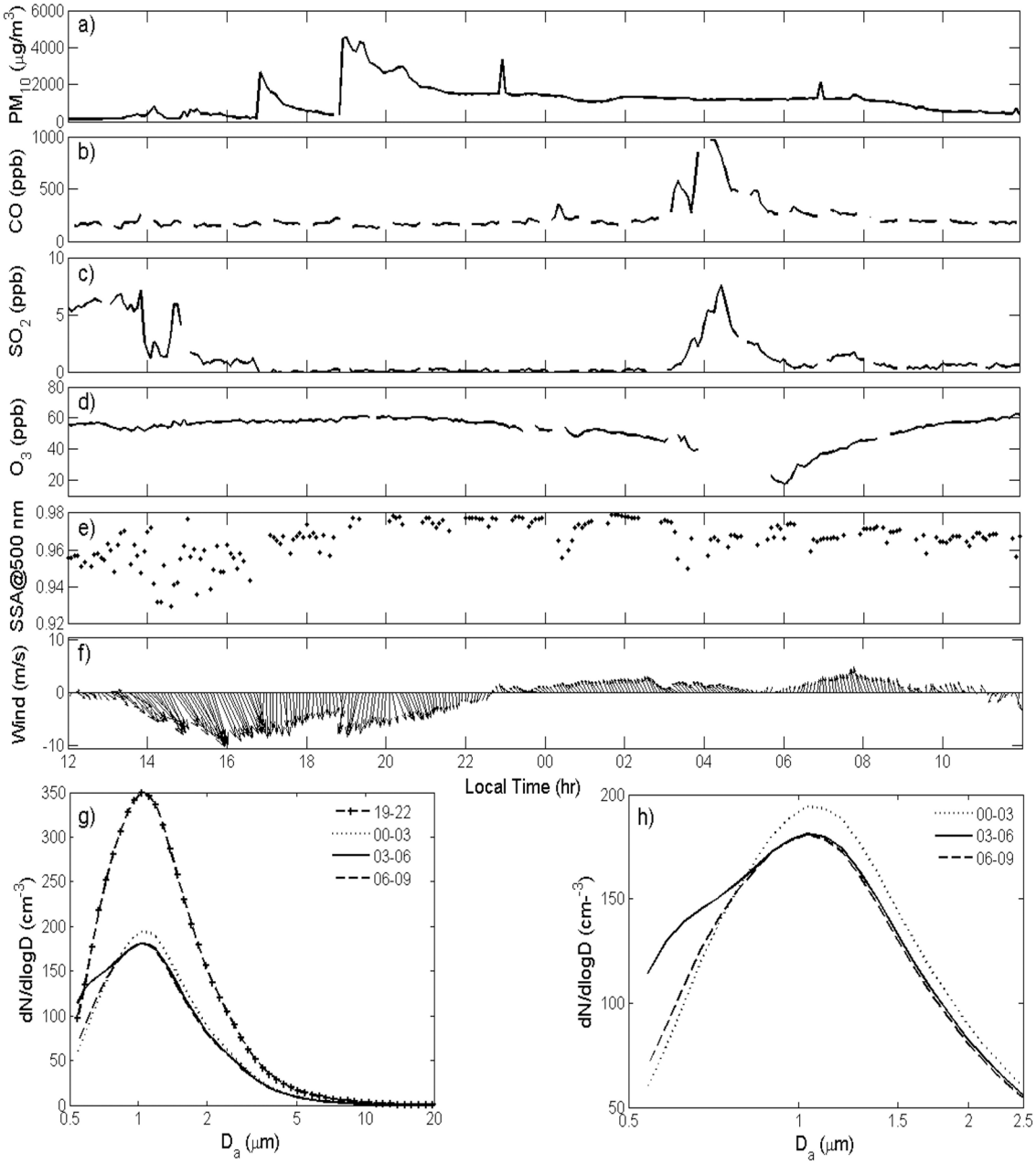

Figure 10. Time series of (a) PM_{10} level, (b) CO, (c) SO_2, (d) O_3, (e) single scattering albedo, and (f) wind vector during a major dust storm on 2–3 May 2008. (g) Average aerosol size distribution during four different periods (time given in the panel) of the dust storm. (h) Aerosol size distribution of fine particles (<2.5 μm) for the latter three periods.

Hexi Corridor, from Dunhuang to the NW to Lanzhou to the SE, and may be of synoptic scale. The spatial coverage and the potential large-scale impact of this dust event will be further studied, with a synergic approach involving satellite data, aerosol model simulation, and radiative transfer modeling. While this particular dust storm is shown as an example here, peaks of gaseous pollutants were observed in most of the several identified dust events. Freshly emitted into the atmosphere over the dust source region, the trace gases and aerosols are likely externally mixed with dust particles. But as anthropogenic pollutants and dust travel together to downwind areas, further interaction is expected and may lead to modification of dust properties. Planning for air quality modeling is underway to simulate the evolution of pollutants and dust along the transport pathway.

4. Conclusions

[39] We have presented the measurements of CO, SO_2, NO_y^*, O_3, aerosol mass concentration (PM_{10}), light scattering coefficient (B_{sp}), light absorption coefficient (B_{ap}), and aerosol size distribution in Zhangye, a rural area near the Gobi deserts in northwestern China, from April to June 2008. The concentrations of primary trace gases for this dust source area

(CO: 265 ± 161 ppb; SO_2: 3.4 ± 4.8 ppb; NO_y^*: 4.2 ± 3.4 ppb) were not as high as observed in eastern China, but comparable to the eastern United States, and indicative of marked influence from anthropogenic emissions. PM_{10} and B_{sp} were substantial at 153 ± 230 $\mu g/m^3$ and 159 ± 191 Mm^{-1}, respectively, due to episodic dust emissions in the region. However, as expected near dust source regions, B_{ap} was comparatively low at 10.3 ± 9.1 Mm^{-1}.

[40] The regular alternation between strong northwest wind in the afternoon and relatively weak southeast wind before dawn was induced by the valley terrain of the area, leading to pronounced diurnal variations in trace gases and aerosols. Low afternoon trace gas levels (CO: ~150 ± 20 ppb; SO_2: ~1.1 ± 1.0 ppb; NO_y^*: ~2.0 ± 2.0 ppb) were associated with strong wind from the desert and active vertical mixing, while the peak gas concentrations (CO: 414 ± 164 ppb; SO_2: 8.1 ± 6.5 ppb; NO_y^*: 7.3 ± 6.7 ppb) appeared in the morning, after overnight accumulation of surface emissions. B_{ap} showed a pattern similar to that of the primary trace gases; the daily maxima (17.8 ± 12.0 Mm^{-1} at 0800 LT, 18.9 ± 13.2 Mm^{-1} at 2100 LT) related to anthropogenic emissions were much higher than the daily low in the afternoon (3.5 ± 1.8 Mm^{-1}). PM_{10} and B_{sp} had less prominent diurnal changes: their peaks during a day (PM_{10}, morning: 194 ± 240 $\mu g/m^3$, evening: 200 ± 413 $\mu g/m^3$; B_{sp}: morning: 202 ± 230 Mm^{-1}; evening: 187 ± 294 Mm^{-1}) were about double of the daily minima at 1400 LT (PM_{10}: 101 ± 80 $\mu g/m^3$; B_{sp}: 72 ± 55 Mm^{-1}). Distinct diurnal variations in aerosol optical properties were observed as well. Dust particles influenced by little pollution had single scattering albedo of 0.95 ± 0.02 in the daytime, and the mixed dust-pollution aerosols featured SSA of 0.91 ± 0.04 at ~0800 LT and 0.89 ± 0.06 at ~2100 LT. The mass scattering efficiency changed from ~0.9 m^2/g in the afternoon to ~1.0 m^2/g in the morning, as aerosol size distribution shifted to submicron particles.

[41] Emissions from diverse local sources in the area were characterized using the ambient measurements during the experiment. In the morning, small coal-burning point sources such as nearby factories probably had a large impact, as suggested by several pollutant spikes. The measurement-derived CO/SO_2, CO/NO_y, NO_y/SO_2, and BC/CO ratios for these sources were 24.6–54.2, 25.8–35.9, 0.79–1.31, and 4.1–6.1 × 10^{-3}, respectively. The same ratios for the industrial sources in the area, estimated in the 2006 INTEX-B emission inventory [*Zhang et al.*, 2009], were 43.7–71.9, 23.7–25.7, 1.84–2.79, and 3.4–4.0 × 10^{-3}. While the comparison may suggest a possible overestimate of NO_x and uncertainties in other species, the results need to be interpreted with caution due to large uncertainty in the measurement-derived ratios and the emission inventory, as well as the sampling mismatch between the two. Local emission sources observed at night demonstrate more diverse properties: the CO/SO_2, CO/NO_y^*, NO_y^*/SO_2, and BC/CO ratios for nighttime pollutant peaks were 10.4–116.7, 21.5–155.9, 0.12–2.29, and 2.6–12 × 10^{-3}, respectively. More field experiments are needed to better characterize the anthropogenic emission sources in the region, and to reduce uncertainties in the emission inventory.

[42] Besides the mixing between dust and pollutants regularly observed at night, we also looked into episodic regional dust storms that could potentially influence large areas. During one strong dust storm on 2–3 May, a nighttime pollutant plume with up to 1000 ppb CO and 8 ppb SO_2, probably from residential sources, was observed at the Zhangye site. The anthropogenic aerosols emitted along with the trace gases mixed with dust particles, causing the SSA to drop from 0.98 to 0.95, and detectable change in aerosol size distribution. Elevated pollutant levels were also observed in several other dust events during the experiment. The mixing between pollution and dust could be ubiquitous over the area, where local and nearby dust emissions frequently encounter anthropogenic emissions. Initially, external mixing is more likely between fresh anthropogenic pollutants and dust. Once driven away from the source area, further interaction between pollutants and dust can possibly modify the optical and hygroscopic properties of the dust particles, key factors determining their effects on radiation, clouds, and biogeochemical cycles.

[43] In summary, our results indicate that substantial anthropogenic air pollutants exist in the Hexi Corridor and can mix with dust particles regularly at night or during strong dust episodes. The dust sometimes moves out of this source region already associated with pollutants, in some cases as much as several ppb of SO_2 and ~1 ppm of CO. The observed nontrivial amount of soot near the deserts may also enhance the light absorption by dust particles. Dust storms passing over cities (e.g., the Zhangye city) and industrial districts in the area may possess even higher levels of pollutants. Anthropogenic emissions in this important dust source region, bound to further increase as the economy and population continue to grow in the future, may play a crucial role in the chemistry and large-scale impact of Asian dust. For the uninhabited desert areas in NW China, the anthropogenic impact on dust composition is likely still small. Further study is necessary to estimate the fraction of the dust leaving northwestern China already mixed with pollutants, and our findings merit more extensive measurements in this region.

[44] **Acknowledgments.** We thank Jianrong Bi, Xianjie Cao, Jinsen Shi, Songtao Song, and Jiliang Xu of Lanzhou University for their help during the field experiment. We also thank two anonymous reviewers for their insightful comments that helped improve the original manuscript. This research was partially supported by MOST (2006CB403706), DOE (DEFG0208ER64571), and NASA (NNG04GE79G, NNX08AH71G).

References

Anderson, T. L., and J. A. Ogren (1998), Determining aerosol radiative properties using the TSI 3563 Integrating Nephelometer, *Aerosol Sci. Technol.*, *29*, 57–69, doi:10.1080/02786829808965551.

Anderson, T. L., et al. (1996), Performance characteristics of a high-sensitivity, three-wavelength, total scatter/backscatter nephelometer, *J. Atmos. Oceanic Technol.*, *13*, 967–986.

Anderson, T. L., S. J. Masonis, D. S. Covert, N. C. Ahlquist, S. G. Howell, A. D. Clarke, and C. S. McNaughton (2003), Variability of aerosol optical properties derived from in situ aircraft measurements during ACE-Asia, *J. Geophys. Res.*, *108*(D23), 8647, doi:10.1029/2002JD003247.

Arimoto, R., X. Y. Zhang, B. J. Huebert, C. H. Kang, D. L. Savoie, J. M. Prospero, S. K. Sage, C. A. Schloesslin, H. M. Khaing, and S. N. Oh (2004), Chemical composition of atmospheric aerosols from Zhenbeitai, China, and Gosan, South Korea, during ACE-Asia, *J. Geophys. Res.*, *109*, D19S04, doi:10.1029/2003JD004323.

Arimoto, R., et al. (2006), Characterization of Asian dust during ACE-Asia, *Global Planet. Change*, *52*, 23–56, doi:10.1016/j.gloplacha.2006.02.013.

Arnott, W. P., K. Hamasha, H. Moosmüller, P. J. Sheridan, and J. A. Ogren (2005), Towards aerosol light-absorption measurements with a 7-wavelength Aethalometer: Evaluation with a photoacoustic instrument and 3-wavelength nephelometer, *Aerosol Sci. Technol.*, *39*, 17–29, doi:10.1080/027868290901972.

Arya, S. P. (1999), *Air Pollution Meteorology and Dispersion*, 310 pp., Oxford Univ. Press, New York.

Baron, P. A., and K. Willeke (2001), *Aerosol Measurement: Principles, Techniques, and Applications*, 2nd ed., 1144 pp., John Wiley, Hoboken, N. J.

Bergin, M., et al. (2001), Aerosol radiative, physical, and chemical properties in Beijing during June 1999, *J. Geophys. Res.*, *106*(D16), 17,969–17,980, doi:10.1029/2001JD900073.

Bian, H., and C. S. Zender (2003), Mineral dust and global tropospheric chemistry: Relative roles of photolysis and heterogeneous uptake, *J. Geophys. Res.*, *108*(D21), 4672, doi:10.1029/2002JD003143.

Bishop, J. K., R. E. Davis, and J. R. Sherman (2002), Robotic observations of dust storm enhancement of carbon biomass in the North Pacific, *Science*, *298*, 817–821, doi:10.1126/science.1074961.

Cao, J. J., S. C. Lee, X. Y. Zhang, J. C. Chow, Z. S. An, K. F. Ho, J. G. Watson, K. Fung, Y. Q. Wang, and Z. X. Shen (2005), Characterization of airborne carbonate over a site near Asian dust source regions during spring 2002 and its climatic and environmental significance, *J. Geophys. Res.*, *110*, D03203, doi:10.1029/2004JD005244.

Carrico, C. M., P. Kus, M. J. Rood, P. K. Quinn, and T. S. Bates (2003), Mixtures of pollution, dust, sea salt, and volcanic aerosol during ACE-Asia: Radiative properties as a function of relative humidity, *J. Geophys. Res.*, *108*(D23), 8650, doi:10.1029/2003JD003405.

Chaudhry, Z., J. V. Martins, Z. Li, S.-C. Tsay, H. Chen, P. Wang, T. Wen, C. Li, and R. R. Dickerson (2007), In situ measurements of aerosol mass concentration and radiative properties in Xianghe, southeast of Beijing, *J. Geophys. Res.*, *112*, D23S90, doi:10.1029/2007JD009055.

Cheng, T., D. Lu, G. Wang, and Y. Xu (2005), Chemical characteristics of Asian dust aerosol from Hunshan Dake sandland in northern China, *Atmos. Environ.*, *39*, 2903–2911, doi:10.1016/j.atmosenv.2004.12.045.

Cheng, T., Y. Liu, D. Lu, Y. Xu, and H. Li (2006), Aerosol properties and radiative forcing in Hunshan Dake desert, northern China, *Atmos. Environ.*, *40*, 2169–2179, doi:10.1016/j.atmosenv.2005.11.054.

Chow, J. C., P. Doraiswamy, J. G. Watson, L.-W. A. Chen, S. S. H. Ho, and D. A. Sodeman (2008), Advances in integrated and continuous measurements for particle mass and chemical composition, *J. Air Waste Manage. Assoc.*, *58*, 141–163, doi:10.3155/1047-3289.58.2.141.

Chu, P. C., Y. Chen, and S. Lu (2008), Atmospheric effects on winter SO_2 pollution in Lanzhou, China, *Atmos. Res.*, *89*, 365–373, doi:10.1016/j.atmosres.2008.03.008.

Dickerson, R. R., and A. C. Delany (1988), Modification of a commercial gas filter correlation CO detector for enhanced sensitivity, *J. Atmos. Oceanic Technol.*, *5*, 424–431, doi:10.1175/1520-0426(1988)005<0424:MOACGF>2.0.CO;2.

Dickerson, R. R., D. H. Stedman, and A. C. Delany (1982), Direct measurements of ozone and nitrogen dioxide photolysis rates in the troposphere, *J. Geophys. Res.*, *87*(C7), 4933–4946, doi:10.1029/JC087iC07p04933.

Dickerson, R. R., A. C. Delany, and A. F. Wartburg (1984), Further modification of a commercial NO_x detector for high sensitivity, *Rev. Sci. Instrum.*, *55*(12), 1995–1998, doi:10.1063/1.1137694.

Du, Y. (2008), New consolidation of emission and processing for air quality modeling assessment in Asia, Master's thesis, 87 pp., Univ. of Tenn. at Knoxville, Knoxville.

Duce, R. A., C. K. Unni, B. J. Ray, J. M. Prospero, and J. T. Merrill (1980), Long-range atmospheric transport of soil dust from Asia to the tropical North Pacific: Temporal variability, *Science*, *209*, 1522–1524, doi:10.1126/science.209.4464.1522.

Dunlea, E. J., et al. (2007), Evaluation of nitrogen dioxide chemiluminescence monitors in a polluted urban environment, *Atmos. Chem. Phys.*, *7*, 2691–2704, doi:10.5194/acp-7-2691-2007.

Fang, M., M. Zheng, F. Wang, K. S. Chim, and S. C. Kot (1999), The long-range transport of aerosols from northern China to Hong Kong—A multi-technique study, *Atmos. Environ.*, *33*, 1803–1817, doi:10.1016/S1352-2310(98)00318-5.

Fehsenfeld, F. C., et al. (1987), A ground-based intercomparison of NO, NO_x, NO_y measurement techniques, *J. Geophys. Res.*, *92*(D12), 14,710–14,722, doi:10.1029/JD092iD12p14710.

Fu, J. S., Y. Du, and Y. F. Lam (2009), 2006 updated Asian emission input for CMAQ fine resolution simulation, paper presented at Air and Waste Management Conference, Air and Waste Manage. Assoc., Detroit, Mich.

Fu, P., J. Huang, C. Li, and S. Zhong (2008), The properties of dust aerosol and reducing tendency of the dust storms in northwest China, *Atmos. Environ.*, *42*, 5896–5904, doi:10.1016/j.atmosenv.2008.03.041.

Gao, Y., R. Arimoto, R. A. Duce, X. Y. Zhang, G. Y. Zhang, Z. S. An, L. Q. Chen, M. Y. Zhou, and D. Y. Gu (1997), Temporal and spatial distributions of dust and its deposition to the China Sea, *Tellus, Ser. B*, *49*, 172–189.

Gao, Y., J. R. Anderson, and X. Hua (2007), Dust characteristics over the North Pacific observed through shipboard measurements during the ACE-Asia experiment, *Atmos. Environ.*, *41*, 7907–7922, doi:10.1016/j.atmosenv.2007.06.060.

Geng, H., Y. Park, H. Hwang, S. Kang, and C.-U. Ro (2009), Elevated nitrogen-containing particles observed in Asian dust aerosol samples collected at the marine boundary layer of the Bohai Sea and the Yellow Sea, *Atmos. Chem. Phys.*, *9*, 6933–6947, doi:10.5194/acp-9-6933-2009.

Ginoux, P., M. Chin, I. Tegen, J. M. Prospero, B. Holben, O. Dubovik, and S.-J. Lin (2001), Sources and distributions of dust aerosols simulated with the GOCART model, *J. Geophys. Res.*, *106*(D17), 20,255–20,273, doi:10.1029/2000JD000053.

Guo, J., K. A. Rahn, and G. Zhuang (2004), A mechanism for the increase of pollution elements in dust storms in Beijing, *Atmos. Environ.*, *38*, 855–862, doi:10.1016/j.atmosenv.2003.10.037.

Guo, Z., Z. Li, J. Farquhar, A. J. Kaufman, N. Wu, C. Li, R. R. Dickerson, and P. Wang (2010), Identification of sources and formation processes of atmospheric sulfate by sulfur Isotope and SEM Measurements, *J. Geophys. Res.*, *115*, D00K07, doi:10.1029/2009JD012893.

Hsu, N. C., S.-C. Tsay, M. D. King, and J. R. Herman (2006), Deep blue retrievals of Asian aerosol properties during ACE-Asia, *IEEE Trans. Geosci. Remote Sens.*, *44*, 3180–3195, doi:10.1109/TGRS.2006.879540.

Hsu, S.-C., S. C. Liu, R. Arimoto, T.-H. Liu, Y.-T. Huang, F. Tsai, F.-J. Lin, and S.-J. Kao (2009), Dust deposition to the East China Sea and its biogeochemical implications, *J. Geophys. Res.*, *114*, D15304, doi:10.1029/2008JD011223.

Huang, J., P. Minnis, B. Lin, T. Wang, Y. Yi, Y. Hu, S. Sun-Mack, and K. Ayers (2006a), Possible influences of Asian dust aerosols on cloud properties and radiative forcing observed from MODIS and CERES, *Geophys. Res. Lett.*, *33*, L06824, doi:10.1029/2005GL024724.

Huang, J., B. Lin, P. Minnis, T. Wang, X. Wang, Y. Hu, Y. Yi, and J. K. Ayers (2006b), Satellite-based assessment of possible dust aerosols semi-direct effect on cloud water path over East Asia, *Geophys. Res. Lett.*, *33*, L19802, doi:10.1029/2006GL026561.

Huang, J., P. Minnis, B. Chen, Z. Huang, Z. Liu, Q. Zhao, Y. Yi, and J. K. Ayers (2008), Long-range transport and vertical structure of Asian dust from CALIPSO and surface measurements during PACDEX, *J. Geophys. Res.*, *113*, D23212, doi:10.1029/2008JD010620.

Huang, K., G. Zhuang, J. Li, Q. Wang, Y. Sun, Y. Lin, and J. S. Fu (2010a), Mixing of Asian dust with pollution aerosol and the transformation of aerosol components during the dust storm over China in spring 2007, *J. Geophys. Res.*, *115*, D00K13, doi:10.1029/2009JD013145.

Huang, K., G. Zhuang, Y. Lin, J. Li, Y. Sun, W. Zhang, and J. S. Fu (2010b), Relation between optical and chemical properties of dust aerosol over Beijing, China, *J. Geophys. Res.*, *115*, D00K16, doi:10.1029/2009JD013212.

Huang, Z., J. Huang, J. Bi, G. Wang, W. Wang, Q. Fu, Z. Li, S.-C. Tsay, and J. Shi (2010), Dust aerosol vertical structure measurements using three MPL lidars during 2008 China-US joint dust field experiment, *J. Geophys. Res.*, *115*, D00K15, doi:10.1029/2009JD013273.

Huebert, B. J., T. Bates, P. B. Russell, G. Shi, Y. J. Kim, K. Kawamura, G. Carmichael, and T. Nakajima (2003), An overview of ACE-Asia: Strategies for quantifying the relationships between Asian aerosols and their climatic impacts, *J. Geophys. Res.*, *108*(D23), 8633, doi:10.1029/2003JD003550.

Husar, R., et al. (2001), Asian dust events of April 1998, *J. Geophys. Res.*, *106*(D16), 18,317–18,330, doi:10.1029/2000JD900788.

Kelly, J. T., C. C. Chuang, and S. W. Anthony (2007), Influence of dust composition on cloud droplet formation, *Atmos. Environ.*, *41*, 2904–2916, doi:10.1016/j.atmosenv.2006.12.008.

Kim, D.-H., B. J. Sohn, T. Nakajima, and T. Takamura (2005), Aerosol radiative forcing over East Asia determined from ground-based solar radiation measurements, *J. Geophys. Res.*, *110*, D10S22, doi:10.1029/2004JD004678.

Kurosaki, Y., and M. Mikami (2003), Recent frequent dust events and their relation to surface wind in East Asia, *Geophys. Res. Lett.*, *30*(14), 1736, doi:10.1029/2003GL017261.

Laskin, A., T. W. Wietsma, B. J. Krueger, and V. H. Grassian (2005), Heterogeneous chemistry of individual mineral dust particles with nitric acid: A combined CCSEM/EDX, ESEM, and ICP-MS study, *J. Geophys. Res.*, *110*, D10208, doi:10.1029/2004JD005206.

Laurent, B., B. Marticorena, G. Bergametti, and F. Mei (2006), Modeling mineral dust emissions from Chinese and Mongolian deserts, *Global Planet. Change*, *52*, 121–141, doi:10.1016/j.gloplacha.2006.02.012.

Leaitch, W. R., et al. (2009), Evidence for Asian dust effects from aerosol plume measurements during INTEX-B 2006 near Whistler, BC, *Atmos. Chem. Phys.*, *9*, 3523–3546, doi:10.5194/acp-9-3523-2009.

Lee, C.-T., M.-T. Chuang, C.-C. Chan, T.-J. Cheng, and S.-L. Huang (2006), Aerosol characteristics from the Taiwan aerosol supersite in the

Asian yellow-dust periods of 2002, *Atmos. Environ.*, *40*, 3409–3418, doi:10.1016/j.atmosenv.2005.11.068.

Lee, K. H., Z. Li, M. S. Wong, J. Xin, Y. Wang, W.-M. Hao, and F. Zhao (2007), Aerosol single scattering albedo estimated across China from a combination of ground and satellite measurements, *J. Geophys. Res.*, *112*, D22S15, doi:10.1029/2007JD009077.

Leighton, P. A. (1961), *Photochemistry of Air Pollution*, 300 pp., Academic, San Diego, Calif.

Li, C., L.T. Marufu, R. R. Dickerson, Z. Li, T. Wen, Y. Wang, P. Wang, H. Chen, and J. W. Stehr (2007), In situ measurements of trace gases and aerosol optical properties at a rural site in northern China during East Asian Study of Tropospheric Aerosols: An International Regional Experiment 2005, *J. Geophys. Res.*, *112*, D22S04, doi:10.1029/2006JD007592.

Li, J., G. Zhuang, K. Huang, Y. Lin, C. Xu, and S. Yu (2008a), Characteristics and sources of air-borne particulate in Urumqi, China, the upstream area of Asia dust, *Atmos. Environ.*, *42*, 776–787, doi:10.1016/j.atmosenv.2007.09.062.

Li, J., et al. (2008b), The chemistry of heavy haze over Urumqi, central Asia, *J. Atmos. Chem.*, *61*(1), 57–72, doi:10.1007/s10874-009-9124-7.

Li, Z., et al. (2007), Preface to special section on East Asian Studies of Tropospheric Aerosols: An International Regional Experiment (EAST-AIRE), *J. Geophys. Res.*, *112*, D22S00, doi:10.1029/2007JD008853.

Liao, H., P. J. Adams, S. H. Chung, J. H. Seinfeld, L. J. Mickley, and D. J. Jacob (2003), Interactions between tropospheric chemistry and aerosols in a unified general circulation model, *J. Geophys. Res.*, *108*(D1), 4001, doi:10.1029/2001JD001260.

Liu, T.-H., F. Tsai, S.-C. Hsu, C.-W. Hsu, C.-J. Shiu, W.-N. Chen, and J.-Y. Tu (2009), Southeastward transport of Asian dust: Source, transport and its contributions to Taiwan, *Atmos. Environ.*, *43*, 458–467, doi:10.1016/j.atmosenv.2008.07.066.

Liu, X., Z.-Y. Yin, X. Zhang, and X. Yang (2004), Analyses of the spring dust storm frequency of northern China in relation to antecedent and concurrent wind, precipitation, vegetation, and soil moisture conditions, *J. Geophys. Res.*, *109*, D16210, doi:10.1029/2004JD004615.

Luke, W. T. (1997), Evaluation of a commercial pulsed fluorescence detector for the measurement of low-level SO_2 concentrations during the Gas-Phase Sulfur Intercomparison Experiment, *J. Geophys. Res.*, *102*(D13), 16,255–16,265, doi:10.1029/96JD03347.

Madronich, S. (1987), Intercomparison of NO_2 photodissociation and U.V. radiometer measurements, *Atmos. Environ.*, *21*, 569–578, doi:10.1016/0004-6981(87)90039-4.

Maxwell-Meier, K., R. Weber, C. Song, D. Orsini, Y. Ma, G. R. Carmichael, and D. G. Streets (2004), Inorganic composition of fine particles in mixed mineral dust–pollution plumes observed from airborne measurements during ACE-Asia, *J. Geophys. Res.*, *109*, D19S07, doi:10.1029/2003JD004464.

McKendry, I. G., A. M. Macdonald, W. R. Leaitch, A. van Donkelaar, Q. Zhang, T. Duck, and R. V. Martin (2008), Trans-Pacific dust events observed at Whistler, British Columbia during INTEX-B, *Atmos. Chem. Phys.*, *8*, 6297–6307, doi:10.5194/acp-8-6297-2008.

Meskhidze, N., W. L. Chameides, and A. Nenes (2005), Dust and pollution: A recipe for enhanced ocean fertilization?, *J. Geophys. Res.*, *110*, D03301, doi:10.1029/2004JD005082.

National Bureau of Statistics of China (2008), *China Statistical Yearbook 2008*, China Stat., Beijing.

Patashnick, H., and E. G. Rupprecht (1991), Continuous PM-10 measurements using the Tapered Element Oscillating Microbalance, *J. Air Waste Manage. Assoc.*, *41*, 1079–1083.

Peters, T. M., and D. Leith (2003), Concentration measurement and counting efficiency of the aerodynamic particle sizer 3321, *J. Aerosol Sci.*, *34*, 627–634, doi:10.1016/S0021-8502(03)00030-2.

Poulida, O., K. L. Civerolo, and R. R. Dickerson (1994), Observations and tropospheric chemistry in central North Carolina, *J. Geophys. Res.*, *99*(D5), 10,553–10,563, doi:10.1029/94JD00404.

Prospero, J. M., P. Ginoux, O. Torres, S. E. Nicholson, and T. E. Gill (2002), Environmental characterization of global sources of atmospheric soil dust identified with the Nimbus 7 Total Ozone Mapping Spectrometer (TOMS) absorbing aerosol product, *Rev. Geophys.*, *40*(1), 1002, doi:10.1029/2000RG000095.

Qian, W., L. Quan, and S. Shi (2002), Variations of the dust storm in China and its climatic control, *J. Clim.*, *15*, 1216–1229, doi:10.1175/1520-0442(2002)015<1216:VOTDSI>2.0.CO;2.

Ro, C.-U., H. Hwang, H. Kim, Y. Chun, and R. Van Grieken (2005), Single-particle characterization of four "Asian dust" samples collected in Korea, using low-*Z* particle electron probe X-ray microanalysis, *Environ. Sci. Technol.*, *39*, 1409–1419, doi:10.1021/es049772b.

Seinfeld, J. H., and S. N. Pandis (1998), *Atmospheric Chemistry and Physics: From Air Pollution to Climate Change*, 1326 pp., John Wiley, Hoboken, N. J.

Shao, Y., and C. H. Dong (2006), A review on East Asian dust storm climate, modeling, and monitoring, *Global Planet. Change*, *52*, 1–22, doi:10.1016/j.gloplacha.2006.02.011.

Shao, Y., et al. (2003), Northeast Asian dust storms: Real-time numerical prediction and validation, *J. Geophys. Res.*, *108*(D22), 4691, doi:10.1029/2003JD003667.

Shen, Z., J. J. Cao, R. Arimoto, Z. Han, R. Zhang, Y. Han, S. Liu, T. Okuda, S. Nakao, and S. Tanaka (2009), Ionic composition of TSP and $PM_{2.5}$ during dust storms and air pollution episodes at Xi'an, China, *Atmos. Environ.*, *43*, 2911–2918, doi:10.1016/j.atmosenv.2009.03.005.

Shetter, R. E., et al. (2003), Photolysis frequency of NO_2: Measurement and modeling during the International Photolysis Frequency Measurement and Modeling Intercomparison (IPMMI), *J. Geophys. Res.*, *108*(D16), 8544, doi:10.1029/2002JD002932.

Solmon, F., P. Y. Chuang, N. Meskhidze, and Y. Chen (2009), Acidic processing of mineral dust iron by anthropogenic compounds over the North Pacific Ocean, *J. Geophys. Res.*, *114*, D02305, doi:10.1029/2008JD010417.

Song, C. H., K. Maxwell-Meier, R. J. Weber, V. Kapustin, and A. Clarke (2005), Dust composition and mixing state inferred from airborne composition measurements during ACE-Asia C130 Flight #6, *Atmos. Environ.*, *39*, 359–369, doi:10.1016/j.atmosenv.2004.08.046.

Stehr, J. W., R. R. Dickerson, K. A. Hallock-Waters, B. G. Doddridge, and D. Kirk (2000), Observations of NO_y, CO, and SO_2 and the origin of reactive nitrogen in the eastern United States, *J. Geophys. Res.*, *105*(D3), 3553–3563, doi:10.1029/1999JD900998.

Streets, D. G., et al. (2003), An inventory of gaseous and primary aerosol emissions in Asia in the year 2000, *J. Geophys. Res.*, *108*(D21), 8809, doi:10.1029/2002JD003093.

Sullivan, R. C., S. A. Guazzotti, D. A. Sodeman, and K. A. Prather (2007), Direct observations of the atmospheric processing of Asian mineral dust, *Atmos. Chem. Phys.*, *7*, 1213–1236, doi:10.5194/acp-7-1213-2007.

Sullivan, R. C., M. J. K. Moore, M. D. Petters, S. M. Kreidenweis, G. C. Roberts, and K. A. Prather (2009), Effect of chemical mixing state on the hygroscopicity and cloud nucleation properties of calcium mineral dust particles, *Atmos. Chem. Phys.*, *9*, 3303–3316, doi:10.5194/acp-9-3303-2009.

Sun, J., M. Zhang, and T. Liu (2001), Spatial and temporal characteristics of dust storms in China and its surrounding regions, 1960–1999: Relations to source area and climate, *J. Geophys. Res.*, *106*(D10), 10,325–10,333, doi:10.1029/2000JD900665.

Sun, Y., G. Zhuang, Y. Wang, X. Zhao, J. Li, Z. Wang, and Z. An (2005), Chemical composition of dust storms in Beijing and implications for the mixing of mineral aerosol with pollution aerosol on the pathway, *J. Geophys. Res.*, *110*, D24209, doi:10.1029/2005JD006054.

Sun, Y., et al. (2010), Asian dust over northern China and its impact on the downstream aerosol chemistry in 2004, *J. Geophys. Res.*, *115*, D00K09, doi:10.1029/2009JD012757.

Ta, W., C. Wei, and F. Chen (2005), Long-term measurements of SO_2 dry deposition over Gansu Province, China, *Atmos. Environ.*, *39*, 7095–7105, doi:10.1016/j.atmosenv.2005.08.018.

Tanaka, T. Y., and M. Chiba (2006), A numerical study of the contributions of dust source regions to the global dust budget, *Global Planet. Change*, *52*, 88–104, doi:10.1016/j.gloplacha.2006.02.002.

Tang, Y., et al. (2004), Impacts of dust on regional tropospheric chemistry during the ACE-Asia experiment: A model study with observations, *J. Geophys. Res.*, *109*, D19S21, doi:10.1029/2003JD003806.

Tobo, Y., D. Z. Zhang, N. Nakata, M. Yamada, H. Ogata, K. Hara, and Y. Iwasaka (2009), Hygroscopic mineral dust particles as influenced by chlorine chemistry in the marine atmosphere, *Geophys. Res. Lett.*, *36*, L05817, doi:10.1029/2008GL036883.

Wang, T., et al. (2004), Relationships of trace gases and aerosols and the emission characteristics at Lin'an, a rural site in eastern China during spring 2001, *J. Geophys. Res.*, *109*, D19S05, doi:10.1029/2003JD004119.

Wang, Y., G. Zhuang, A. Tang, W. Zhang, Y. Sun, Z. Wang, and Z. An (2007), The evolution of chemical components of aerosols at five monitoring sites of China during dust storms, *Atmos. Environ.*, *41*, 1091–1106, doi:10.1016/j.atmosenv.2006.09.015.

Xia, X.-A., H.-B. Chen, P.-C. Wang, X.-M. Zong, J.-H. Qiu, and P. Gouloub (2005), Aerosol properties and their spatial and temporal variations over North China in spring 2001, *Tellus, Ser. B*, *57*, 28–39.

Xu, J., M. H. Bergin, X. Yu, G. Liu, J. Zhao, C. M. Carrico, and K. Baumann (2002), Measurement of aerosol chemical, physical and radiative properties in the Yangtze delta region of China, *Atmos. Environ.*, *36*, 161–173, doi:10.1016/S1352-2310(01)00455-1.

Xu, J., M. H. Bergin, R. Greenwald, J. J. Schauer, M. M. Shafer, J. L. Jaffrezo, and G. Aymoz (2004), Aerosol chemical, physical, and radiative characteristics near a desert source region of northwest China during ACE-Asia, *J. Geophys. Res.*, *109*, D19S03, doi:10.1029/2003JD004239.

Xuan, J., G. Liu, and K. Du (2000), Dust emission inventory in northern China, *Atmos. Environ.*, *34*, 4565–4570, doi:10.1016/S1352-2310(00)00203-X.

Yan, H. (2007), Aerosol scattering properties in northern China, *Atmos. Environ.*, *41*, 6916–6922, doi:10.1016/j.atmosenv.2007.04.052.

Yan, P., J. Tang, J. Huang, J. T. Mao, X. J. Zhou, Q. Liu, Z. F. Wang, and H. G. Zhou (2008), The measurement of aerosol optical properties at a rural site in northern China, *Atmos. Chem. Phys.*, *8*, 2229–2242, doi:10.5194/acp-8-2229-2008.

Yuan, H., G. Zhuang, K. A. Rahn, X. Zhang, and Y. Li (2006), Composition and mixing of individual particles in dust and nondust conditions of north China, spring 2002, *J. Geophys. Res.*, *111*, D20208, doi:10.1029/2005JD006478.

Yuan, H., G. Zhuang, J. Li, Z. Wang, and J. Li (2008), Mixing of mineral with pollution aerosols in dust season in Beijing: Revealed by source apportionment study, *Atmos. Environ.*, *42*, 2141–2157, doi:10.1016/j.atmosenv.2007.11.048.

Yue, X., H. Wang, Z. Wang, and K. Fan (2009), Simulation of dust aerosol radiative feedback using the Global Transport Model of Dust: 1. Dust cycle and validation, *J. Geophys. Res.*, *114*, D10202, doi:10.1029/2008JD010995.

Zhang, D., and Y. Iwasaka (2001), Chlorine deposition on dust particles in marine atmosphere, *Geophys. Res. Lett.*, *28*, 3613–3616, doi:10.1029/2001GL013333.

Zhang, D., and Y. Iwasaka (2004), Size change of Asian dust particles caused by sea salt interaction: Measurements in southwestern Japan, *Geophys. Res. Lett.*, *31*, L15102, doi:10.1029/2004GL020087.

Zhang, D., Y. Iwasaka, G. Shi, J. Zang, M. Hu, and C. Li (2005), Separated status of the natural dust plume and polluted air masses in an Asian dust storm event at coastal areas of China, *J. Geophys. Res.*, *110*, D06302, doi:10.1029/2004JD005305.

Zhang, K., and H. Gao (2007), The characteristics of Asian-dust storms during 2000–2002: From the source to the sea, *Atmos. Environ.*, *41*, 9136–9145, doi:10.1016/j.atmosenv.2007.08.007.

Zhang, Q., et al. (2009), Asian emissions in 2006 for the NASA INTEX-B mission, *Atmos. Chem. Phys.*, *9*, 5131–5153, doi:10.5194/acp-9-5131-2009.

Zhang, X. Y., S. L. Gong, R. Arimoto, Z. X. Shen, F. M. Mei, D. Wang, and Y. Cheng (2003a), Characterization and temporal variation of Asian dust aerosol from a site in the northern Chinese deserts, *J. Atmos. Chem.*, *44*, 241–257, doi:10.1023/A:1022900220357.

Zhang, X. Y., S. L. Gong, Z. X. Shen, F. M. Mei, X. X. Xi, L. C. Liu, Z. J. Zhou, D. Wang, Y. Q. Wang, and Y. Cheng (2003b), Characterization of soil dust aerosol in China and its transport and distribution during 2001 ACE-Asia: 1. Network observations, *J. Geophys. Res.*, *108*(D9), 4261, doi:10.1029/2002JD002632.

Zhang, X. Y., Y. Q. Wang, X. C. Zhang, W. Guo, T. Niu, S. L. Gong, Y. Yin, P. Zhao, J. L. Jin, and M. Yu (2008), Aerosol monitoring at multiple locations in China: Contribution of EC and dust to aerosol light absorption, *Tellus, Ser. B*, *60*, 647–656.

Zhang, Y., and G. R. Carmichael (1999), The role of mineral aerosol in tropospheric chemistry in East Asia—A model study, *J. Appl. Meteorol.*, *38*, 353–366, doi:10.1175/1520-0450(1999)038<0353:TROMAI>2.0.CO;2.

Zhang, Y., Y. Sunwoo, V. Kotamarthi, and G. R. Carmichael (1994), Photochemical oxidant processes in the presence of dust: An evaluation of the impact of dust on particulate nitrate and ozone formation, *J. Appl. Meteorol.*, *33*, 813–824, doi:10.1175/1520-0450(1994)033<0813:POPITP>2.0.CO;2.

Zhao, T. L., S. L. Gong, X. Y. Zhang, and D. A. Jaffe (2008), Asian dust storm influence on North American ambient PM levels: Observational evidence and controlling factors, *Atmos. Chem. Phys.*, *8*, 2717–2728, doi:10.5194/acp-8-2717-2008.

Zhu, C., B. Wang, and W. Qian (2008), Why do dust storms decrease in northern China concurrently with the recent global warming?, *Geophys. Res. Lett.*, *35*, L18702, doi:10.1029/2008GL034886.

Zou, X. K., and P. M. Zhai (2004), Relationship between vegetation coverage and spring dust storms over northern China, *J. Geophys. Res.*, *109*, D03104, doi:10.1029/2003JD003913.

S. W. Bell, Science Systems and Applications Inc., Lanham, MD 20706, USA.

H. Chen, Institute of Atmospheric Physics, Chinese Academy of Sciences, Beijing 100029, China.

R. R. Dickerson, Q. Ji, C. Li, and Z. Li, Earth System Science Interdisciplinary Center, University of Maryland, College Park, MD 20742, USA. (can.li@nasa.gov)

J. S. Fu and Y. Gao, Department of Civil and Environmental Engineering, University of Tennessee, Knoxville, TN 37996, USA.

J. Huang and W. Zhang, College of Atmospheric Sciences, Lanzhou University, Lanzhou 730000, China.

S.-C. Tsay, NASA Goddard Space Flight Center, Greenbelt, MD 20770, USA.